Article

Cell Metabolism

12-Lipoxygenase Regulates Cold Adaptation and Glucose Metabolism by Producing the Omega-3 Lipid 12-HEPE from Brown Fat

Graphical Abstract

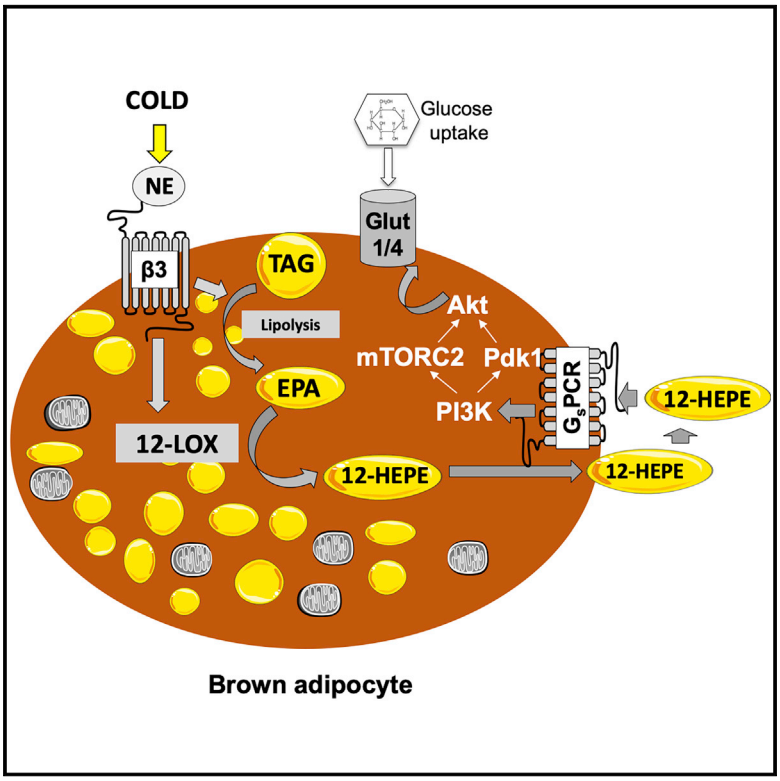

Authors

Luiz Osório Leiria, Chih-Hao Wang, Matthew D. Lynes, ..., Michael A. Kiebish, Matthew Spite, Yu-Hua Tseng

Correspondence

yu-hua.tseng@joslin.harvard.edu

In Brief

Leiria et al. uncover a cold-induced response involving the activation of the enzyme 12-lipoxygenase in brown adipose tissue, which subsequently produces an omega-3 oxylipin 12-HEPE to promote glucose uptake into tissue via an insulin-like intracellular signaling pathway.

Highlights

- Cold exposure increases 12-LOX activity in brown adipose tissue
- 12-LOX activity in BAT contributes to cold adaptation
- 12-HEPE is a cold-induced and BAT-secreted oxylipin
- 12-HEPE promotes glucose uptake *in vivo* and *in vitro*

Leiria et al., 2019, Cell Metabolism *30*, 768–783
October 1, 2019
https://doi.org/10.1016/j.cmet.2019.07.001

CellPress

CellPress

Cell Metabolism
Article

12-Lipoxygenase Regulates Cold Adaptation and Glucose Metabolism by Producing the Omega-3 Lipid 12-HEPE from Brown Fat

Luiz Osório Leiria,[1] Chih-Hao Wang,[1] Matthew D. Lynes,[1] Kunyan Yang,[1] Farnaz Shamsi,[1] Mari Sato,[1] Satoru Sugimoto,[1] Emily Y. Chen,[3] Valerie Bussberg,[3] Niven R. Narain,[3] Brian E. Sansbury,[4] Justin Darcy,[1] Tian Lian Huang,[1] Sean D. Kodani,[1] Masaji Sakaguchi,[1] Andréa L. Rocha,[11] Tim J. Schulz,[1,12] Alexander Bartelt,[8,9,10] Gökhan S. Hotamisligil,[8] Michael F. Hirshman,[1] Klaus van Leyen,[7] Laurie J. Goodyear,[1] Matthias Blüher,[6] Aaron M. Cypess,[5] Michael A. Kiebish,[3] Matthew Spite,[4] and Yu-Hua Tseng[1,2,13,*]

[1]Joslin Diabetes Center, Section on Integrative Physiology and Metabolism, Harvard Medical School, Boston, MA, USA
[2]Harvard Stem Cell Institute, Harvard University, Cambridge, MA, USA
[3]BERG, Framingham, MA, USA
[4]Center for Experimental Therapeutics and Reperfusion Injury, Department of Anesthesiology, Perioperative, and Pain Medicine, Brigham and Women's Hospital and Harvard Medical School, Boston, MA, USA
[5]National Institutes of Health, Bethesda, MD, USA
[6]Department of Medicine, University of Leipzig, Leipzig, Germany
[7]Massachusetts General Hospital, Harvard Medical School, Neuroprotection Research Laboratory, Department of Radiology, Charlestown, MA, USA
[8]Department of Genetics and Complex Diseases & Sabri Ülker Center, Harvard T.H. Chan School of Public Health, Boston, MA, USA
[9]Institute for Cardiovascular Prevention (IPEK), Ludwig-Maximilians-University, Munich 80336, Germany
[10]German Center for Cardiovascular Research (DZHK), Partner Site Munich Heart Alliance, Munich, Germany
[11]Department of Biochemistry and Tissue Biology, Institute of Biology, State University of Campinas, Campinas, Brazil
[12]Department of Adipocyte Development and Nutrition, German Institute of Human Nutrition, Potsdam-Rehbrücke, Germany
[13]Lead Contact
*Correspondence: yu-hua.tseng@joslin.harvard.edu
https://doi.org/10.1016/j.cmet.2019.07.001

SUMMARY

Distinct oxygenases and their oxylipin products have been shown to participate in thermogenesis by mediating physiological adaptations required to sustain body temperature. Since the role of the lipoxygenase (LOX) family in cold adaptation remains elusive, we aimed to investigate whether, and how, LOX activity is required for cold adaptation and to identify LOX-derived lipid mediators that could serve as putative cold mimetics with therapeutic potential to combat diabetes. By utilizing mass-spectrometry-based lipidomics in mice and humans, we demonstrated that cold and β3-adrenergic stimulation could promote the biosynthesis and release of 12-LOX metabolites from brown adipose tissue (BAT). Moreover, 12-LOX ablation in mouse brown adipocytes impaired glucose uptake and metabolism, resulting in blunted adaptation to the cold *in vivo*. The cold-induced 12-LOX product 12-HEPE was found to be a batokine that improves glucose metabolism by promoting glucose uptake into adipocytes and skeletal muscle through activation of an insulin-like intracellular signaling pathway.

INTRODUCTION

The prevalence of obesity and metabolic syndrome has reached pandemic levels worldwide and has been gradually increasing over the last few decades (GBD 2015 Obesity Collaborators, 2017). Several epidemiologic studies have identified high body mass index (BMI) as a risk factor for many chronic diseases, including cardiovascular disease and diabetes mellitus (Singh et al., 2013; Roberto et al., 2015), illustrating the urgency for identifying novel molecular targets and therapeutic strategies to treat these metabolic disorders. Due to the high capacity of brown adipose tissue (BAT) in consuming glucose and fatty acids to generate heat and expend energy (Cannon and Nedergaard,

Context and Significance

Brown adipose tissue (BAT) maintains body temperature in response to cold by burning blood glucose and fatty acids. Understanding how BAT clears blood glucose is of importance for developing new therapeutic approaches to combat diabetes. In this study, the authors find that cold stress activates the enzyme 12-lipoxygenase (12-LOX) in BAT, which produces lipids that help to maintain body temperature. Deletion of 12-LOX from mouse BAT inhibits the production of 12-HEPE, a 12-LOX-derived lipid that can shuttle glucose into tissues and improve glucose tolerance in obese mice.

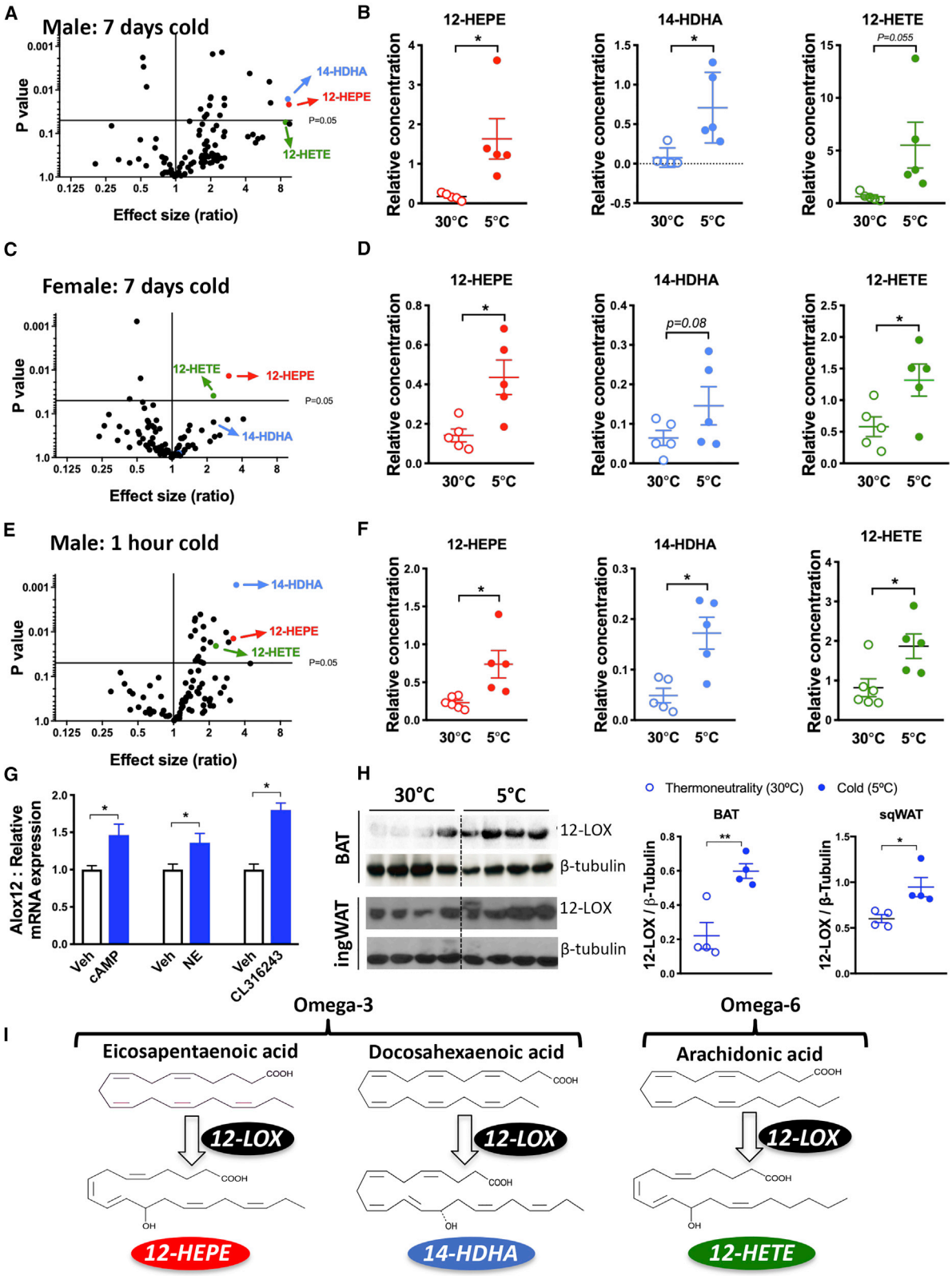

Figure 1. Cold Exposure Induces 12-LOX-Derived Lipid Secretion into the Circulation

(A) Volcano plot of serum lipids profiled in male C57BL6/J mice exposed to 5°C or 30°C for 7 days. Effect size (ratio) means $\log_2$ (fold change 5°C versus 30°C).

(legend continued on next page)

2004; Bartelt et al., 2011; Townsend and Tseng, 2014) and the presence of BAT in adult humans (Nedergaard et al., 2007; Cypess et al., 2009; van Marken Lichtenbelt et al., 2009; Virtanen et al., 2009), increasing the amount or activity of functional BAT has been considered an appealing approach for the treatment or prevention of obesity and related metabolic diseases.

Cold exposure elevates BAT volume and activity, thus increasing energy expenditure and whole-body insulin sensitivity and facilitating weight loss in obese humans (van der Lans et al., 2013; Yoneshiro et al., 2013; Hanssen et al., 2015). Furthermore, the second type of thermogenic adipose tissue called beige or brite (brown-in-white) fat is activated by cold or adrenergic stimuli (Frontini and Cinti, 2010). Thermogenic fat serves as a "metabolic sink" by consuming glucose and fatty acids from the circulation (Frontini and Cinti, 2010; Kajimura et al., 2015). The high metabolic capacity of thermogenic fat is mediated by a tightly controlled transcriptional and post-transcriptional regulatory system (Seale et al., 2008; Chouchani et al., 2016; Lynes et al., 2017; Bartelt et al., 2018). Although brown/beige fat has attracted attention as a potential target for treating metabolic diseases because of its energy-dissipating function, at least part of its beneficial effect is actually due to its secretory function, and consequent capacity to affect metabolic functions in other tissues such as muscle, white fat, and liver (Stanford et al., 2013; Wang et al., 2014). Thermogenic adipocytes can synthesize and release factors such as peptides, lipids, or other metabolites called batokines and can directly or indirectly support thermogenesis (Wang et al., 2015; Chen et al., 2016; Villarroya et al., 2017). These secreted factors may act as endocrine, paracrine, or autocrine agents to regulate a number of physiological functions required for adaptive thermogenesis (Wang et al., 2015; Villarroya et al., 2017). The identification of novel BAT-secreted molecules that may work as cold mimetics to promote substrate metabolism is essential to uncover pathways that can serve as new therapeutic targets for metabolic diseases, including diabetes.

Cold increases the expression and activity of enzymes that catalyze lipid oxidation (Lynes et al., 2017). A cluster of oxidized lipid metabolites called oxylipins are derived from omega-3 or omega-6 polyunsaturated fatty acids (PUFAs) and can regulate a number of metabolic processes, including adipogenesis and fuel utilization (Barquissau et al., 2017). Oxylipins are biosynthesized through the oxidative activity of the cyclooxygenases (COX), lipoxygenases (LOX), or cytochrome P450 epoxygenase (CYP P450) and play well-documented roles in controlling acute inflammation and its resolution (Serhan, 2014; Capdevila et al., 2015; Barquissau et al., 2017). These lipid mediators can also exert metabolic effects required for non-shivering thermogenesis, such as the formation of beige adipocytes by the COX-derived prostaglandins (Vegiopoulos et al., 2010) or the induction of fatty acid uptake into BAT and skeletal muscle by the cold or exercise-induced cytochrome P450 epoxygenase and epoxide hydrolase product (±)12,13-dihydroxy-9Z-octadecenoic acid (12,13-diHOME) (Lynes et al., 2017; Stanford et al., 2018). Considering these studies, the role of LOX enzymes for adaptive thermogenesis remains elusive.

In the present study, we revealed a new function for LOX enzymes and their corresponding lipid metabolites in the adaptive thermogenesis. Using lipidomic profiling of humans and mice, we observed that β3-adrenergic stimulation could promote the biosynthesis and release of BAT-derived metabolites from the enzyme 12-LOX. Importantly, one of the 12-LOX omega-3 metabolites, 12-hydroxyeicosapentaenoic acid (12-HEPE), acts as a paracrine and/or endocrine factor to promote glucose uptake into brown fat and muscle. The ablation of 12-LOX *in vitro* impairs the glucose-uptake capacity of brown adipocytes. Importantly, *in vivo* CRISPR-Cas9-mediated deletion of 12-LOX, specifically in BAT, hampers the animal's capacity to adapt to cold temperature. These findings uncover a new role for lipoxygenases and their oxylipin products in the regulation of glucose metabolism and adaptive thermogenesis in both mice and humans.

RESULTS

Cold Exposure or β3-Adrenergic Stimulation Increase Circulating Levels of 12-LOX-Derived Lipids in Mice and Humans

The use of lipidomics technologies, combined with appropriate genetic models, has helped to identify lipid mediators that serve as metabolic messengers to communicate energy status and modulate fuel utilization among tissues (Cao et al., 2008; Liu et al., 2013; Yore et al., 2014; Lynes et al., 2017). Aiming to search for LOX products that reflect the activity of this family of enzymes under cold condition, we used liquid chromatography coupled with tandem mass spectrometry (LC-MS/MS) to measure the concentrations of a panel of 88 oxidized lipids in the serum of mice that were housed in cold (5°C) or thermoneutrality (30°C) for 7 days. Interestingly, we found a coordinated elevation of three 12-LOX metabolites, namely 12-HEPE, 14-hydroxydocosahexaenoic acid (14-HDHA), and 12-hydroxyeicosatetraenoic acid (12-HETE) by cold exposure in both male and female

(B) Serum levels of 12-LOX products 12-HEPE, 14-HDHA, and 12-HETE from male mice exposed to 5°C or 30°C for 7 days (n = 5).
(C) Volcano plot of serum lipids profiled in female C57BL6/J mice exposed to 30°C or 5°C for 7 days. Effect size (ratio) means $\log_2$ (fold change 5°C versus 30°C).
(D) Serum levels of 12-LOX products 12-HEPE, 14-HDHA, and 12-HETE from female mice exposed to 5°C or 30°C for 7 days (n = 5).
(E) Volcano plot of serum lipids profiled in male C57BL6/J mice exposed to 5°C or room temperature (22°C) for 1 h . Effect size (ratio) means $\log_2$ (fold change 5°C versus 22°C).
(F) Serum levels of 12-LOX products 12-HEPE, 14-HDHA, and 12-HETE from male mice exposed to 5°C or 22°C for 1 h (n = 5).
(G) Alox12 mRNA expression in differentiated WT-1 brown adipocytes stimulated with cyclic AMP (cAMP, 1 mM), norepinephrine (NE, 1 μM), or CL316,243 (1 μM) for 4 h.
(H) Western blot analysis of 12-LOX protein in BAT and ingWAT from mice housed at 5°C or 30°C for 7 days (n = 4). β-tubulin serves as the loading control. Right panels: quantifiction of 12-LOX relative to β-tubulin.
(I) Scheme illustrating the biosynthetic pathways by which 12-HEPE, 14-HDHA, and 12-HETE are derived from their polyunsaturated fatty acid precursors EPA, DHA, and AA.
For all panels, *$p < 0.05$, unpaired student's t test. Data are represented as mean ± SEM.
All the lipid quantification data were detected using non-targeted lipidomics; thus, relative values are shown. See also Figure S1.

C57BL6/J mice (Figures 1A–1D). Omega-3 or -6 PUFAs, mainly eicosapentaenoic acid (EPA), docosahexaenoic acid (DHA), and arachidonic acid (AA), can be oxidized by 12-LOX to produce 12-HEPE, 14-HDHA, and 12-HETE, respectively (Hamberg, 1980; Brash, 1999; Serhan et al., 2009; Kuhn et al., 2015) (Figure 1I). Notably, the levels of HEPEs, HDHAs, and HETEs derived from other LOX subtypes, COXs, or CYP450 were not modified by cold, except for a reduction in 5-LOX products, 5-HEPE, and 5-HETE (Figures S1A and S1B). Since acute cold exposure activates brown fat glucose and fatty acid uptake (van Marken Lichtenbelt et al., 2009; Virtanen et al., 2009; Bartelt et al., 2011; Lynes et al., 2017), we sought to measure serum lipid levels after short-term cold exposure and found that the levels of 12-LOX metabolites were elevated after only 1 h of cold exposure (Figures 1E and 1F). Circulating levels of other HEPEs, HDHAs, and HETEs were not altered, except for a small increase in 9-HEPE, which is a product of non-enzymatic oxidation (Figure S1C). To quantify the circulating concentrations of these lipid mediators, we performed a targeted lipidomics analysis. We found the serum levels of 12-HEPE, 14-HDHA and 12-HETE were around 50, 15, and 25 nMol for male C57BL/6 mice housed for 7 days in thermoneutrality (Figure S1D).

The coordinated regulation of 12-LOX products by cold exposure prompted us to examine whether cold and/or β3-adrenergic activation is capable of inducing the expression of 12-LOX in brown or beige adipocytes. While 12-LOX (*Alox12*) is known to biosynthesize lipid metabolites such as 12(*S*)-HEPE, 14(S)-HDHA, and 12(*S*)-HETE, 15-LOX (*Alox15*, also known as 12/15-LOX) is able to produce both 12- and 15-LOX products in mice such as 12(*S*)-HETE and 15(*S*)-HETE from AA and 15(*S*)-HEPE from EPA (Brash, 1999; Kuhn et al., 2015). The 12R-LOX enzyme, which is encoded by the *Alox12b* gene, is responsible for the biosynthesis of the *R* stereoisomers 12(*R*)-HETE and 12(*R*)-HEPE (Brash, 1999; Kuhn et al., 2015). Since brown and beige fat are the primary fat depots activated by cold stimulation, we measured the expression of genes encoding these enzymes in BAT and inguinal white adipose tissue (ingWAT) to determine which lipoxygenase is expressed and could potentially be activated in these tissues. We found negligible levels of mRNA expression of *Alox15*, *Alox15b*, and *Alox12b* (Ct > 32 when measured by qRT-PCR; note that Ct is a relative and not absolute quantification), while *Alox12* was expressed at a substantially higher level in BAT and ingWAT (Ct ca. 26–27). These data suggest that the *S* stereoisomers were the ones being produced under cold. *Alox12* mRNA expression was elevated in differentiated brown adipocytes in response to three different adrenergic mimetics, namely cAMP dibutyrate, norepinephrine (NE), and the β3-adrenergic receptor agonist CL316,243 (Figure 1G). We found that 12-LOX protein expression was significantly higher in both BAT and ingWAT of mice housed in 5°C for 7 days than mice kept at 30°C (Figure 1H), although at the mRNA level, *Alox12* mRNA was elevated in BAT but not in ingWAT (Figure S1E). *Alox12* mRNA levels were not altered in either BAT or ingWAT after 1 h in 5°C (Figure S1E), indicating that upon an acute cold challenge, it is the enzymatic activity, rather than the transcriptional modulation, of 12-LOX that contributes to the production of the metabolites. Furthermore, we found that within the adipose tissue, the cold-induced 12-LOX mRNA expression predominantly occurred in mature adipocytes but not in stromal vascular fraction SVF (Figure S1F).

Lipolysis in response to acute cold or adrenergic stimulation leads to increased availability of free fatty acids to serve as substrates for oxidative metabolism and also contributes to the release of lipid metabolites into the circulation (Haemmerle et al., 2006). To determine whether lipolysis was required for the biosynthesis and secretion of 12-LOX products upon short-term cold exposure, we measured circulating lipid levels in mice with adipose-specific deletion of adipose triglyceride lipase (ATGL) (Adipoq^{CRE}/Atgl^{flox}). ATGL is the major lipase that hydrolyzes triglyceride in adipose tissue (Ahmadian et al., 2011). As previously reported (Ahmadian et al., 2011; Schreiber et al., 2017; Shin et al., 2017), these animals displayed cold intolerance and an increased BAT mass due to brown fat whitening (Figures S1G–S1I). We found that the cold-induced elevation of 12-LOX lipid metabolites was abolished or significantly reduced in the Adipoq^{CRE}/Atgl^{flox} mice (Figure S1J), indicating that the activation of the ATGL-dependent lipolytic pathway in adipose tissue is essential for the production of these circulating lipids in response to acute cold challenge.

Elevation of 12-LOX Metabolites in the Circulation of Humans Acutely Treated with Mirabegron

To further test the hypothesis that adrenergic-induced activation of 12-LOX is relevant in humans, we performed a lipidomics analysis in plasma samples from healthy human subjects treated either with a single oral dose of the specific β3-adrenergic agonist mirabegron (200 mg) or a placebo. As previously reported by Cypess et al. (2015), these subjects exhibited higher ^{18}F-fluorodeoxyglucose (FDG) uptake in BAT and elevated energy expenditure after mirabegron treatment. We detected significantly higher levels of 12-HEPE and 14-HDHA in mirabegron-treated subjects, while 12-HETE was unchanged (Figures 2A and 2B). Importantly, 12-HEPE was the most significantly upregulated lipid metabolite among all the detected lipid species (Figures 2A, 2B, and S2A–S2C). Furthermore, the circulating levels of these lipids positively correlated with BAT activity measured by FDG uptake (Figures 2C–2E).

BAT Is a Source for Cold-Induced 12-LOX Lipid Metabolites

To further assess whether BAT could be the source of the 12-LOX metabolites in response to cold, we measured the circulating oxidized lipid levels in wild-type control mice and in Myf5^{CRE}/BMPr1a^{flox} mice, which are characterized by impaired BMP signaling in brown fat progenitors leading to a severe paucity of BAT (Schulz et al., 2013). Comparing these mice with the wild-type animals allows for the identification of BAT-secreted factors (Figure 3A). The cold-induced increase in circulating 12-HEPE was completely diminished in the Myf5^{CRE}/Bmpr1a^{flox} group, while 14-HDHA was still induced by cold in both groups, and 12-HETE levels were unchanged (Figure 3B).

Next, targeted lipidomic analyses were performed in BAT and ingWAT of C57BL6/J mice housed at 5°C or 30°C for 7 days (Figure 3C). Although 12-HEPE could be detected in both fat depots, its cold-induced biosynthesis was only observed in the interscapular BAT. In contrast, levels of 14-HDHA were increased by cold in both fat depots, and the levels of 12-HETE were not

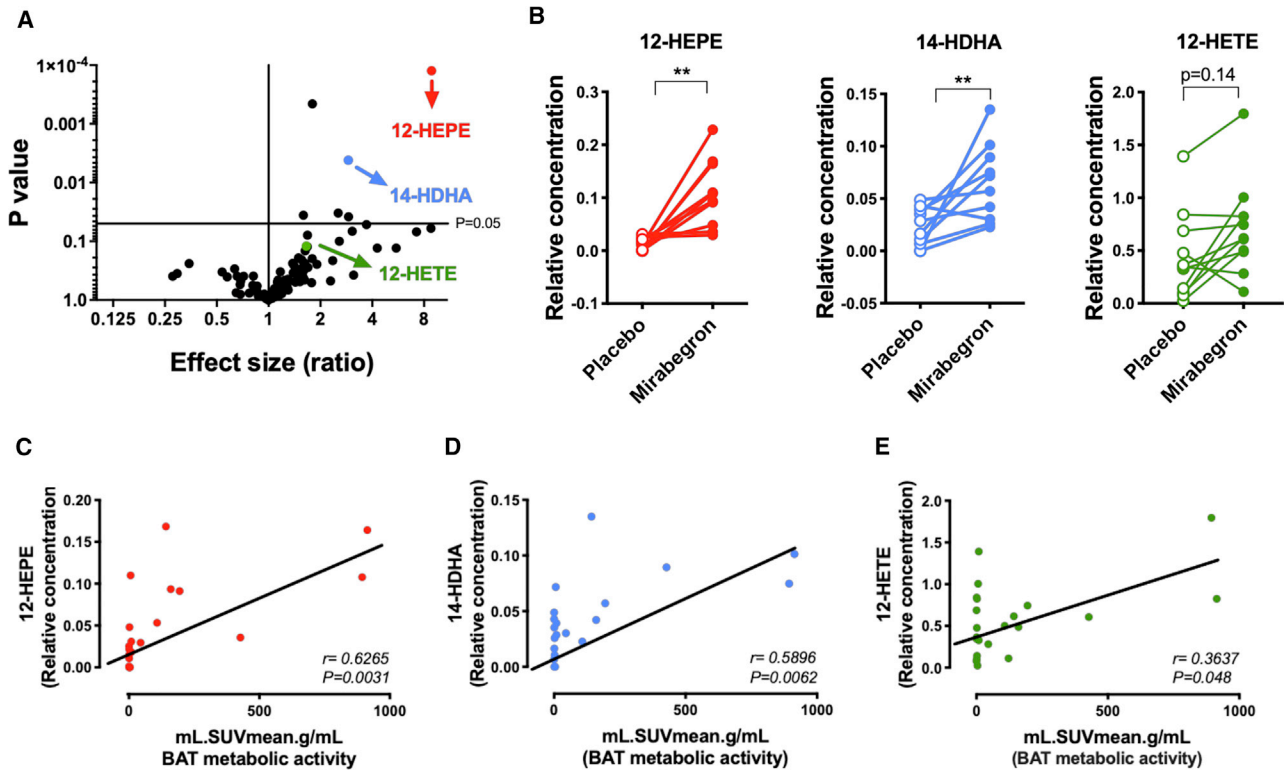

Figure 2. Mirabegron Treatment Increases the Secretion of 12-LOX Metabolites in Human Subjects

(A) Volcano plot of plasma lipids profiled in human subjects treated with a single oral dose of mirabegron (200 mg) or treated with placebo. Effect size (ratio) means $\log_2$ (fold change mirabegron versus placebo).

(B) Circulating levels of the 12-LOX-derived lipids from human subjects treated with placebo or mirabegron (n = 10–11). **p < 0.01, ***p < 0.001. Data are represented as paired individual values.

(C–E) Spearman correlation between circulating 12- LOX metabolite levels and BAT glucose uptake measured by PET

All the lipid quantification data were detected using non-targeted lipidomics; thus, relative values are shown. See also Figure S2.

altered in either tissue (Figure 3D). To validate the capacity of these fat depots to produce lipid metabolites, we dissected BAT and ingWAT from mice exposed to 5°C or 30°C for 7 days and incubated the tissue explants in Krebs-Ringer buffer for 1 h before quantifying lipid concentrations in this buffer. BAT from mice exposed to cold secreted twice as much 12-HEPE as control BAT, while ingWAT secretion was not affected by cold (Figures 3E and 3F). Using this assay, we could not detect significant changes of 14-HDHA and 12-HETE release from BAT or ingWAT in response to cold (Figures 3E and 3F). Since adipose tissue contains multiple cell types, to determine whether these lipid mediators are directly produced by activated brown adipocytes, we used *in vitro* differentiated human and murine brown adipocytes treated with sympathomimetics. We found significantly higher levels of 12-HEPE and 14-HDHA in the media of murine brown adipocytes treated with the β3-adrenergic agonist CL316,243 for 4 h (Figures S3A–S3C). Importantly, this phenomenon was also observed in human brown adipocytes. As shown in Figures 3G and 3H, the levels of all three 12-LOX oxylipins were increased by at least 2-fold in the media of human brown adipocytes treated with forskolin. Together, these findings suggest that brown adipocytes are the cellular source producing 12-LOX metabolites in response to cold or β3-adrenergic stimulation in rodents and humans.

12-LOX Activity in BAT Is Required for Adaptive Thermogenesis

In order to investigate whether 12-LOX activity is required for cold adaptation, we pre-treated C57BL/6 mice with a dual 12- and 12/15-LOX chemical inhibitor (LOXBlock-1) for 30 min and then exposed these animals to 5°C for 4 h. LOXBlock-1 abolished the cold-induced release of 12-LOX products, 12-HEPE and 14-HDHA (Figure 4A), and led to an impairment in cold tolerance, which was prevented by 12(*S*)-HEPE co-injection (Figures 4B and S4A). We observed similar effects using two other distinct 12-LOX inhibitors (Baicalein and NCTT956) (Figures S4B and S4C). The effect of the 12-LOX inhibitors was not due to changes in the expression of thermogenic genes in BAT because the cold-induced levels of thermogenic mRNA such as *Ucp1*, *Dio*$_2$, and *Ppargc1a* were not altered between vehicle and LOXBlock-1-treated groups (Figure S4D), suggesting that the 12-LOX lipid mediators may directly and acutely modulate the activity of brown fat, independent of major transcriptional changes.

To more specifically assess the role of 12-LOX activity in BAT thermogenic capacity and secretory function, we generated brown fat-specific *Alox12* knockout (KO) mice using a combined Cre-lox and CRISPR-Cas9 technology (Platt et al., 2014). We crossed Cre-dependent Rosa26 Cas9 knockin mice (Rosa26-

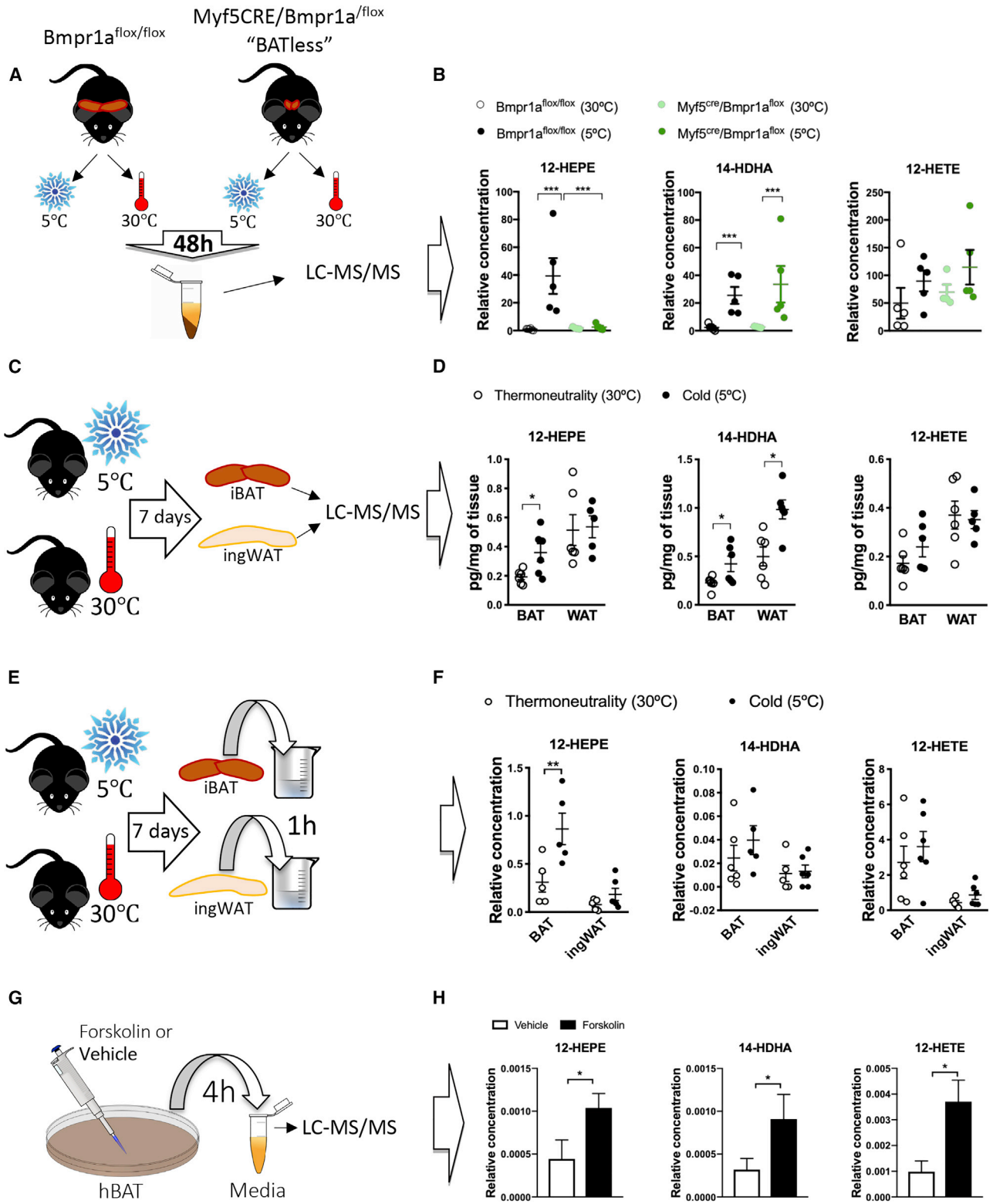

Figure 3. 12-HEPE Is a Cold-Inducible Lipid that Is Biosynthesized in BAT

(A) Schematic panel illustrating the experimental design of the lipidomics performed in serum from Bmpr1a^{flox} (WT) and Myf5^{CRE}/Bmpr1a^{flox} (mice with iBAT paucity) male mice exposed to 30°C or 5°C for 2 days.

(B) Serum lipid levels in male Bmpr1a^{flox} (WT) and Myf5^{CRE}/Bmpr1a^{flox} mice exposed to 30°C or 5°C for 2 days (n = 4–5).

(legend continued on next page)

LSL-Cas9) with Ucp1-Cre animals to generate Ucp1^{CRE}/Cas9 mice (Figure 4C). These mice received bilateral interscapular BAT injections with AAV2/8 expressing either a specific gRNA targeting exon 1 of the *Alox12* gene (Figure S4E) or an empty vector (EV) control (Figure 4C), thus generating UCP1^{CRE}-Alox12 KO mice or EV control mice. We confirmed that the level of 12-LOX protein was diminished in BAT but not in the ingWAT of UCP1^{CRE}-Alox12 KO mice (Figure S4F). UCP1^{CRE}-Alox12 KO mice had no changes in body weight, fasting glucose, or tissue weights when raised at standard room temperature (22°C) (Figures S4G–S4I). Cold-induced elevation of 12-LOX products in circulation was absent in UCP1^{CRE}-Alox12 KO mice after 1-h exposure at 5°C (Figure 4D). Importantly, UCP1^{CRE}-Alox12 KO mice displayed impaired cold adaptation compared to the EV control mice in a cold tolerance test (Figure 4E). In line with these findings, the UCP1^{CRE}-Alox12 KO mice also displayed a significant reduction in whole-body oxygen consumption in response to NE stimulation (Figure 4F). Similar to what was observed in mice treated with LOXBlock-1-treated mice, the levels of cold-stimulated expression of thermogenic genes were comparable between UCP1^{CRE}-Alox12 KO and EV control mice (Figure S4J).

Given that 12-LOX products positively correlated with glucose uptake into BAT from human subjects treated with mirabegron, we hypothesized that the loss of 12-LOX in brown adipocytes would lead to impaired glucose metabolism and mitochondrial activity in brown adipocytes in a cell-autonomous fashion. To test this hypothesis, we generated *Alox12* KO cells by using the CRISPR-Cas9 system and the same gRNA targeting Alox12 that was used for the aforementioned *in vivo* studies (Figure S4K). Indeed, the capacity of Alox12 KO brown adipocytes to take up glucose was impaired compared to EV control cells, while *Alox12* re-expression completely restored basal glucose uptake (Figure 4G). Consistent with these findings, *Alox12*-deficient brown adipocytes displayed a reduced extracellular acidification rate in a glycolysis stress test that was fully restored by the re-expression of *Alox12* (Figure 4H). Next, we investigated whether *Alox12* deletion in brown adipocytes could affect mitochondrial respiration. While basal and uncoupled respiration were unaffected by *Alox12* deletion, the *Alox12* KO brown adipocytes displayed a severe defect in maximal respiration in response to the mitochondrial uncoupler carbonyl cyanide-4-(trifluoromethoxy) phenylhydrazone (FCCP), which was restored by the 12-LOX re-expression (Figure 4I). Although differentiation capacity was unaltered in the 12-LOX KO cells (Figure S4L), expression of selected thermogenic genes, such as *Ucp1* and *Cidea*, but not *Ppargc1a* and *Dio$_2$*, was reduced in the KO cells, which was nominally restored by *Alox12* re-expression (Figure S4M). The inability of 12-LOX re-expression in restoring *Ucp1* and *Cidea* expression in the KO cells and the fact that level of *Ucp1* mRNA was not altered in BAT of UCP1^{CRE}-Alox12 KO mice suggest that 12-LOX might not be directly involved in the transcriptional regulation of *Ucp1* and other thermogenic genes. Therefore, the reduced levels of *UCP1* and *Cidea* in the 12-LOX KO cells might be secondary to other metabolic changes. Taken together, these data indicate that 12-LOX, presumably by generating its downstream lipid metabolites, plays an essential role in BAT-mediated regulation of adaptive thermogenesis and glucose metabolism.

12-HEPE Biosynthesis and Secretion Are Repressed in Obesity

Since brown fat mass and activity are lower in obese patients and are inversely correlated with body mass index (BMI) in humans (van Marken Lichtenbelt et al., 2009; Cypess et al., 2009), we proceeded to determine the relationship between circulating levels of 12-LOX products and metabolic parameters in a cohort of subjects with a broad distribution of BMI. Interestingly, we found significantly lower levels of the 12-LOX metabolites 12-HEPE, 14-HDHA, and 12-HETE in overweight (BMI = 25–30 kg/m^2) and obese subjects (BMI > 30 kg/m^2) compared to lean individuals (BMI < 25 kg/m^2) (Figures 5A–5C). Due to the non-linear relationship with the variants, we used the Spearman's correlation and identified a significant negative correlation between plasma levels of 12-LOX products and BMI (Figures S5A–S5C). Importantly, the levels of these lipids were also negatively correlated with insulin resistance measured by HOMA-IR and circulating leptin levels (Figures 5D–5I); however, these correlations were dependent on BMI.

Because our data suggest that fat depots are potential sources of the circulating 12-LOX metabolites, we measured lipid levels in BAT of diet-induced obese (DIO) mice and control lean mice. We found that the concentration of 12-HEPE was significantly lower in BAT of DIO mice, contrasting with the not significantly altered 14-HDHA and higher 12-HETE levels (Figure S5D).

The 12-LOX-Derived Lipid 12-HEPE Is a Brown-Fat-Secreted Mediator of Glucose Uptake

Because the levels of 12-HEPE were consistently increased by cold in all of the conditions we tested and among the 12-LOX metabolites we detected it was the lipid species consistently found to be produced by BAT and repressed by obesity in murine brown fat and human plasma, we sought to determine whether 12-HEPE is able to regulate energy homeostasis and fuel utilization in DIO mice. DIO mice were treated daily with intraperitoneal

(C) Schematic panel illustrating the experimental design of the lipidomics performed in iBAT and ingWAT harvested from male C57BL6/J mice exposed to 30°C or 5°C for 7 days.

(D) Lipid levels in iBAT and ingWAT from C57BL6/J male mice exposed to 30°C or 5°C for 7 days (n = 5–6). Targeted lipidomics was used for lipid quantification.

(E) Schematic panel illustrating the experimental design of the lipidomics performed in conditioned medium incubated with ingWAT or iBAT explants, harvested from C57BL6/J mice exposed to 30°C or 5°C for 7 days.

(F) Medium lipid levels in Krebs Ringer buffer after its incubation (1 h) with iBAT or ingWAT harvested from C57BL6/J male mice exposed to 30°C or 5°C for 7 days.

(G) Schematic panel illustrating the experimental design of the lipidomics performed in media collected from *in vitro* differentiated human brown adipocytes stimulated with forskolin or vehicle for 4 h.

(H) 12-HEPE, 14-HDHA, and 12-HETE levels in conditioned media of human brown adipocytes stimulated with forskolin or vehicle. *p < 0.05, **p < 0.01, ***p < 0.001. Unpaired Student's t test. n = 5 per group. Data are represented as mean ± SEM.

All the lipid quantification data (except for Figure 3D) were detected using non-targeted lipidomics; thus, relative values are shown. See also Figure S3.

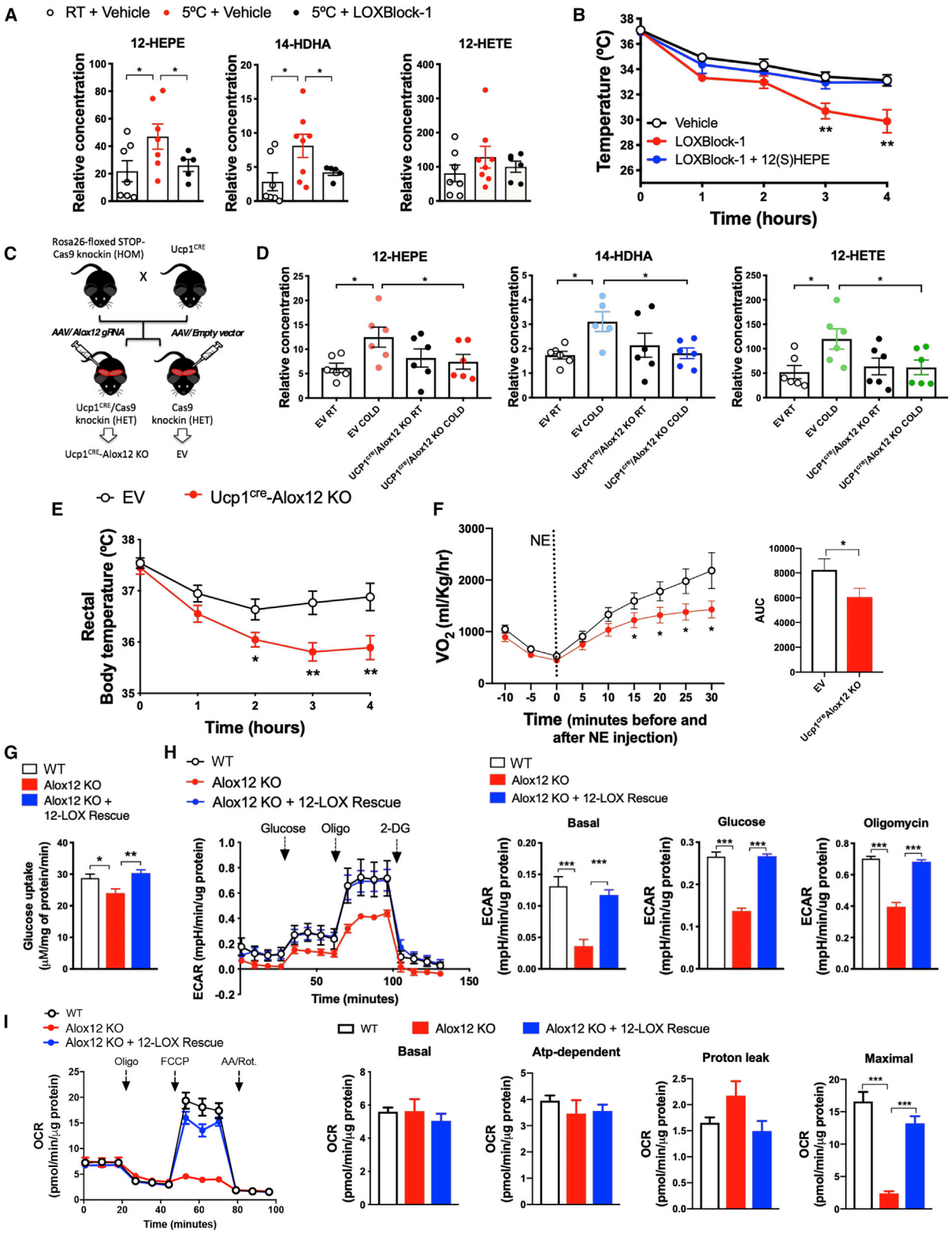

(legend on next page)

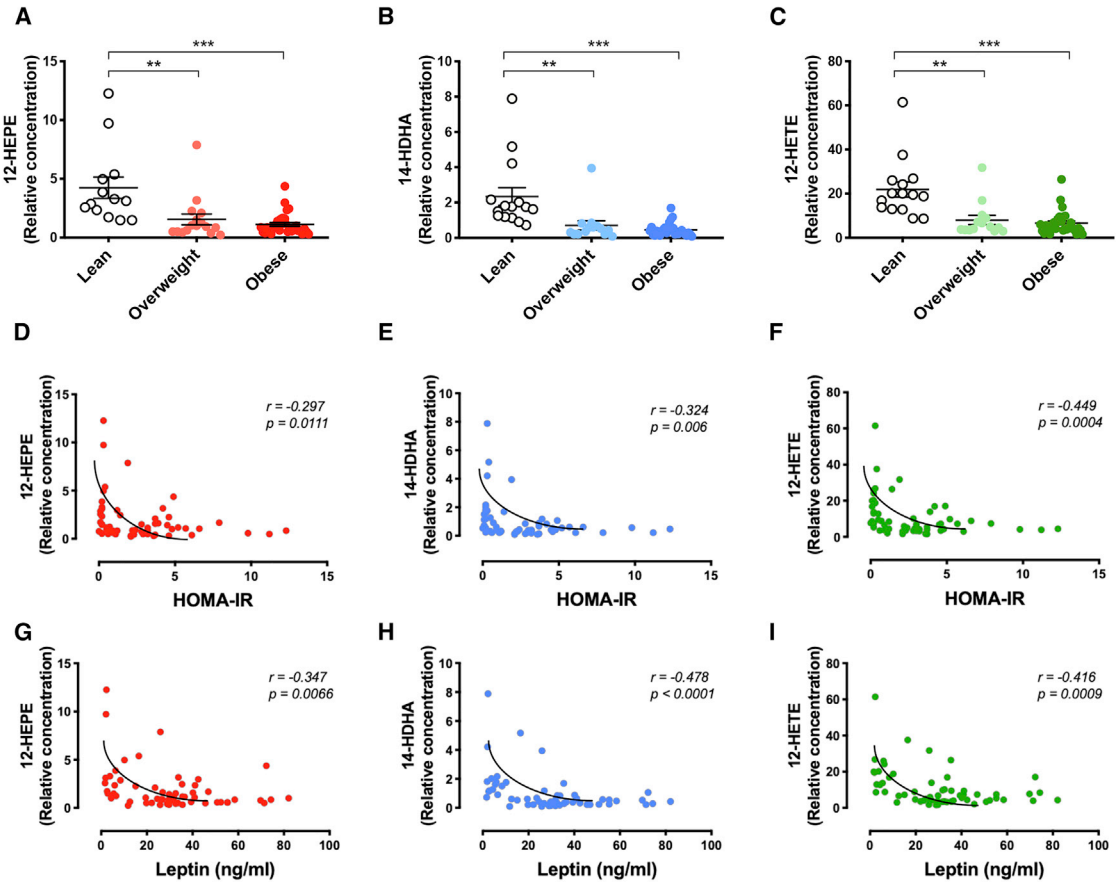

Figure 5. Negative association of Plasma Levels of 12-LOX Metabolites with Obesity and Insulin Resistance in Humans

(A–C) Plasma 12-HEPE, 14-HDHA and 12-HETE levels in lean (BMI < 25 kg/m^2), overweight (BMI > 25 kg/m^2, < 30 kg/m^2), and obese (BMI > 30 kg/m^2) subjects (n = 55). **p < 0.01, ***p < 0.001. Data are represented as mean ± SEM.

(D–F) Spearman correlation between the plasma levels of 12-LOX products and insulin resistance measured by HOMA-IR.

(G–I) Spearman correlation between the plasma levels of 12-LOX products and circulating leptin concentrations.

The lipid quantification data were detected using non-targeted lipidomics; thus, relative values are shown. See also Figure S5.

(i.p.) injections of 12(*S*)-HEPE (200 μg/kg) or PBS for 2 weeks. The i.p. injection increased circulating 12-HEPE levels by 2.5-fold 30 min after treatment (Figure S6A). Although no change in body weight gain or fasting glucose was observed (Figures 6A and 6B), 12(*S*)-HEPE-treated DIO mice displayed a marked improvement in glucose tolerance compared to the vehicle-treated group (Figure 6C). There was no difference in the serum insulin levels before or after glucose injection (Figure S6B), indicating that the effects of 12(*S*)-HEPE did not rely on the regulation of glucose-induced insulin release. Moreover, 12(*S*)-HEPE

Figure 4. 12-LOX Ablation in Brown Adipocytes Impairs Glucose Utilization and Cold Adaptation

(A) Serum lipid levels in C57BL6/J male mice receiving i.p. injection of LOXblock-1 or vehicle (DMSO) for 15 min, and then exposed to 5°C or 22°C for 4 h (n = 6–7).

(B) Rectal temperature during cold tolerance test in C57BL6/J male mice receiving i.p. injection of LOXblock-1 or vehicle (DMSO) in the presence or absence of 12(S)-HEPE (200 μg/kg via i.p.). (n = 5–6).

(C) Schematic panel illustrating the strategy for the generation of Ucp1^{CRE}/Alox12 KO mice using the Ucp1^{CRE} and CRISPR-Cas9 knockin mice.

(D) Serum levels of 12-LOX-derived lipids in the control empty vector (EV) mice and Ucp1^{CRE}/Alox12 KO mice, exposed to 22°C or 5°C for 1 h. (n = 6).

(E) Rectal temperature during cold tolerance test in EV and Ucp1^{CRE}/Alox12 KO male mice (n = 12).

(F) Oxygen consumption measured by CLAMS in EV and Ucp1^{CRE}/Alox12 KO mice receiving i.p. injection of norepinephrine (n = 12). Area under curve (AUC) quantification is shown in the right panel.

(G) Glucose uptake in *in vitro* differentiated wild-type (WT) , Alox12 KO, and 12-LOX re-expressed Alox12 KO brown adipocytes.

(H) Extracellular acidification rate (ECAR) during the glycolysis stress test in *in vitro* differentiated Alox12-KO and 12-LOX re-expressed Alox12 KO brown adipocytes. Quantifications are shown in the right panels.

(I) Oxygen consumption ratio (OCR) during the mitochondrial stress test in *in vitro* differentiated WT, Alox12-KO, and 12-LOX re-expressed Alox12 KO brown adipocytes. Quantifications are shown in the right panels.

*p < 0.05, **p < 0.01, ***p < 0.001. Data are represented as mean ± SEM. The lipid quantification data were detected using non-targeted lipidomics; thus, relative values are shown. See also Figure S4.

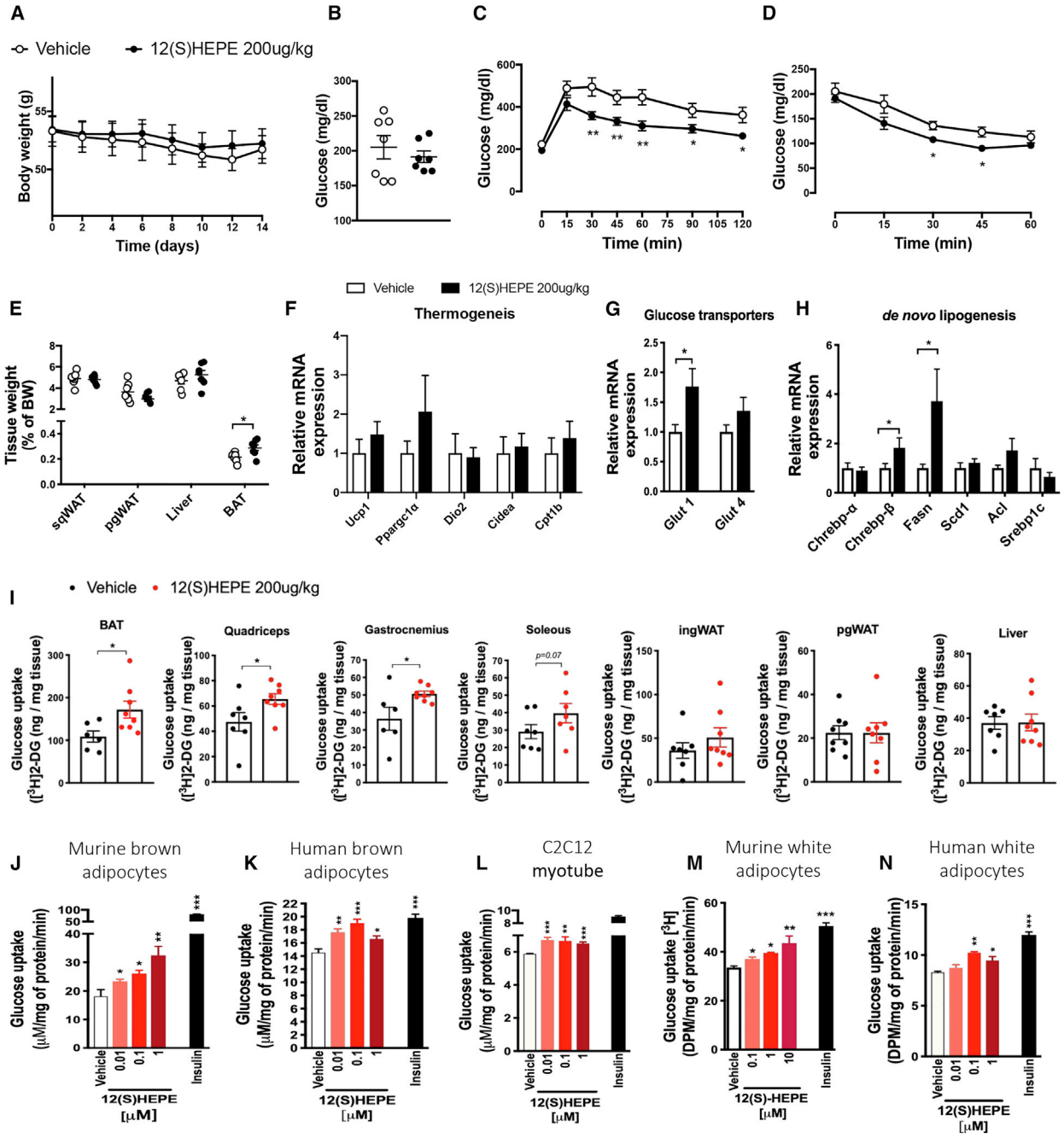

Figure 6. 12-HEPE Regulates Glucose Uptake *in vitro* and *in vivo*

(A) Body weight in 12(S)-HEPE- and vehicle-treated DIO male mice (n = 7).

(B) Fasting serum glucose measured in 12(S)-HEPE- and vehicle-treated DIO mice (n = 7).

(C) Glucose tolerance test (GTT) performed in 6-hr fasted 12(S)-HEPE- and vehicle-treated DIO mice (n = 7).

(D) Insulin tolerance test (ITT) performed in 6-hr fasted 12(S)-HEPE and vehicle-treated DIO mice (n = 7).

(E) Relative tissue weight for pgWAT, ingWAT, liver, and BAT (normalized to body weight) from 12(S)-HEPE- and vehicle-treated DIO mice (n = 7).

(F–H) mRNA expression measured by qPCR for genes related to thermogenic program (F), glucose transport (G), and *de novo* lipogenesis (H) in BAT from 12(S)-HEPE- and vehicle-treated DIO mice (n = 7).

(I) *In vivo* glucose uptake into BAT, ingWAT, pgWAT, quadriceps, gastrocnemius, soleus, and liver of C57BL6/J lean mice reveiging i.v. injection of 12(S)-HEPE or vehicle for 30 min followed by [^{3}H]2-deoxyglucose i.v. injection (n = 6–8).

(J–N) *In vitro* glucose uptake in murine brown adipocytes (J), human brown adipocytes (K), murine myocytes (C2C12) (L), murine white adipocytes (3T3-F442A cells) (M), and human white adipocytes (hWAT) (N) treated with 12(S)-HEPE or vehicle for 30 min followed by addition of [^{3}H]2-deoxyglucose. n = 4–6 technical replicates from at least 2 biological replicate experiments. *p < 0.05, **p < 0.01, ***p < 0.001. Data are represented as mean ± SEM. See also Figure S6.

treatment led to an improvement in insulin sensitivity in DIO mice (Figure 6D). Animals treated with 12(*S*)-HEPE did not show any change in food intake (Figures S6C and S6D), physical activity (Figure S6E), carbon dioxide production (VCO_2), or oxygen consumption (VO_2) (Figures S6F and S6G). There was a trend for an increase in VO_2 and respiratory exchange ratio (Figure S6H). Since the effects of omega-3 PUFAs are associated with their ability to reduce adipose tissue inflammation (Oh et al., 2010; Talukdar et al., 2011; Spite et al., 2014), we examined whether the improved glucose metabolism observed in 12(*S*)-HEPE-treated DIO mice was mediated by alterations in adipose inflammation. The mRNA expression of pro- and anti-inflammatory genes was not altered by 12(*S*)-HEPE treatment in ingWAT, perigonadal white adipose tissue (pgWAT), or BAT, with the exception of increased IL-10 expression in pgWAT of 12(*S*)-HEPE-treated animals (Figures S6I–S6K). We did not observe differences in M1 and M2 macrophage populations in the pgWAT of 12(*S*)-HEPE treated mice compared to the PBS-treated group by flow cytometry analysis (Figure S6L). Interestingly, BAT weight was increased in DIO mice treated with 12(*S*)-HEPE compared to control animals (Figure 6E). Although there was no change in the expression of genes involved in the thermogenic program in the BAT (Figure 6F), 12(*S*)-HEPE treatment increased mRNA expression of the glucose transporter *Glut-1* (Figure 6G), the glucose-sensitive transcription factor *Chrebp-β* and its downstream target fatty acid synthase (*Fasn*) (Figure 6H), suggesting that 12(*S*)-HEPE treatment promotes glucose uptake and utilization in BAT of DIO mice.

To test the hypothesis that 12(*S*)-HEPE improves glucose homeostasis by promoting glucose uptake into tissues, we measured tissue [^{3}H] 2-deoxyglucose ([^{3}H]2-DG) uptake in lean mice acutely treated with 12(*S*)-HEPE. 12(*S*)-HEPE treatment significantly increased [^{3}H]2-DG uptake into BAT and skeletal muscle but not into pgWAT, ingWAT, or liver (Figure 6I). To examine whether 12(*S*)-HEPE regulates glucose uptake in a cell-autonomous manner, we measured [^{3}H]2-DG uptake into different cell types *in vitro*. We found that 12(*S*)-HEPE was able to increase glucose uptake in differentiated murine and human brown adipocytes as well as in C2C12 myotubes (Figures 6J–6L), indicating that 12(*S*)-HEPE could directly regulate glucose uptake in adipocytes and muscle cells. Interestingly, while 12(S)-HEPE did not promote 2-DG uptake into WAT *in vivo*, it could increase glucose uptake into human and mouse white adipocytes differentiated *in vitro* (Figures 6M and 6N). These data suggest that 12-HEPE functions as a mediator of glucose uptake in adipose tissue and skeletal muscle.

12-HEPE Promotes Glucose Uptake by Triggering the PI3K/Akt/Glut Pathway in a G_sPCR-Dependent Fashion

Since the phosphatidylinositol-4,5-bisphosphate 3-kinase (PI3K)/protein kinase B (Akt)/Glut-4 axis is the canonical signaling pathway that regulates glucose uptake, we hypothesized that 12(*S*)-HEPE activates this pathway to promote glucose uptake into tissues. Akt activation is triggered by the phosphorylation at residues Ser473 and/or Thr308 by the mammalian target of rapamycin complex 2 (mTORC2) and phosphoinositide dependent kinase-1 (Pdk-1), respectively (Sarbassov et al., 2005). Interestingly, we found that 12(*S*)-HEPE promoted AKT phosphorylation at both Ser473 and Thr308 in murine brown adipocytes (Figures 7A, S7A, and S7B), indicating co-participation of mTORC2 and Pdk1 in the signaling pathway triggered by 12(*S*)-HEPE. Indeed, in addition to increased mTORC2 phosphorylation at Ser2481, we also observed phosphorylation of the downstream target AS160 at Thr642 in response to 12(*S*)-HEPE stimulation in brown adipocytes (Figures 7A, S7C, and S7D). Importantly, 12(*S*)-HEPE triggered similar signaling cascade *in vivo,* since phosphorylation of Akt (Ser473) and mTOR (Ser2481) was increased in BAT of mice acutely injected with 12(S)-HEPE (i.v., 30 min, 200 μg/kg) (Figures S7E and S7F). To determine whether the mTORC-PI3K-Akt axis plays an essential role in 12(*S*)-HEPE-induced glucose uptake, murine brown adipocytes were pre-treated with inhibitors of mTORC1, mTORC1/2, or PI3K, and the glucose uptake in response to 12(*S*)-HEPE was measured. While the incubation with the mTORC1 inhibitor Rapamycin did not affect glucose uptake, the mTORC1/2 inhibitor Torin1 partially reduced 12(*S*)-HEPE's effect on glucose uptake. Pre-treatment with the PI3K inhibitor Wortmannin almost completely abolished this effect (Figure 7B). Furthermore, Glut4 was translocated to the plasma membrane in response to 12(*S*)-HEPE stimulation in murine brown adipocytes (Figure 7C).

Many lipid mediators exert their effects through stimulation of G-protein-coupled receptors (GPCRs). To identify the class of GPCR that mediates the effect of 12(S)-HEPE on promoting glucose uptake, we performed an *in vitro* glucose-uptake assay in murine brown adipocytes pre-treated with inhibitors of 3 subtypes of GPCR, namely G_q/11, G_i, and G_s protein-coupled receptors. Pretreatment with the G_q/11 and G_i antagonists, YM254890 and pertussis toxin, did not change the 12(S)-HEPE effect (Figures 7D and 7E); however, the G_s inhibitor melittin completely blunted the 12(S)-HEPE-induced glucose uptake (Figure 7F), suggesting that 12(S)-HEPE utilizes a G_sPCR to trigger downstream signaling. To further validate these findings, we knocked down *Gnas*, the gene encoding the stimulatory subunit of G_s protein, in brown adipocytes (Figure S7G) and found that 12(S)-HEPE-induced glucose uptake was abolished in the *Gnas* knockdown cells (Figure 7G). Thus, 12(S)-HEPE exerts the glucose shuttling effect by triggering a G_sPCR, which leads to PI3K-mTORC2-Akt activation and Glut4 translocation to the plasma membrane.

DISCUSSION

Oxylipins are oxidized lipids derived from PUFAs that play important roles in health and disease. Using lipidomics analyses, here, we demonstrate that the 12-LOX biosynthetic pathway is activated in BAT in response to cold or β-adrenergic stimulation, generating oxylipin mediators that are released into the circulation where they can exert glucose shuttling effect on tissues to support thermogenesis. This effect is mediated through the stimulation of a G_sPCR, which triggers an insulin-like signaling pathway that results in Glut4 translocation and glucose uptake into the cell. These data reveal a novel cold-induced 12-LOX-dependent pathway in thermoregulation and fuel utilization.

Among the 12-LOX-derived oxylipins, 12-HETE is the most studied and characterized lipid (Nunemaker et al., 2008; Ma et al., 2010; Cole et al., 2013; Tersey et al., 2014). To date, 12-LOX is described as a potential mediator in the pathogenesis

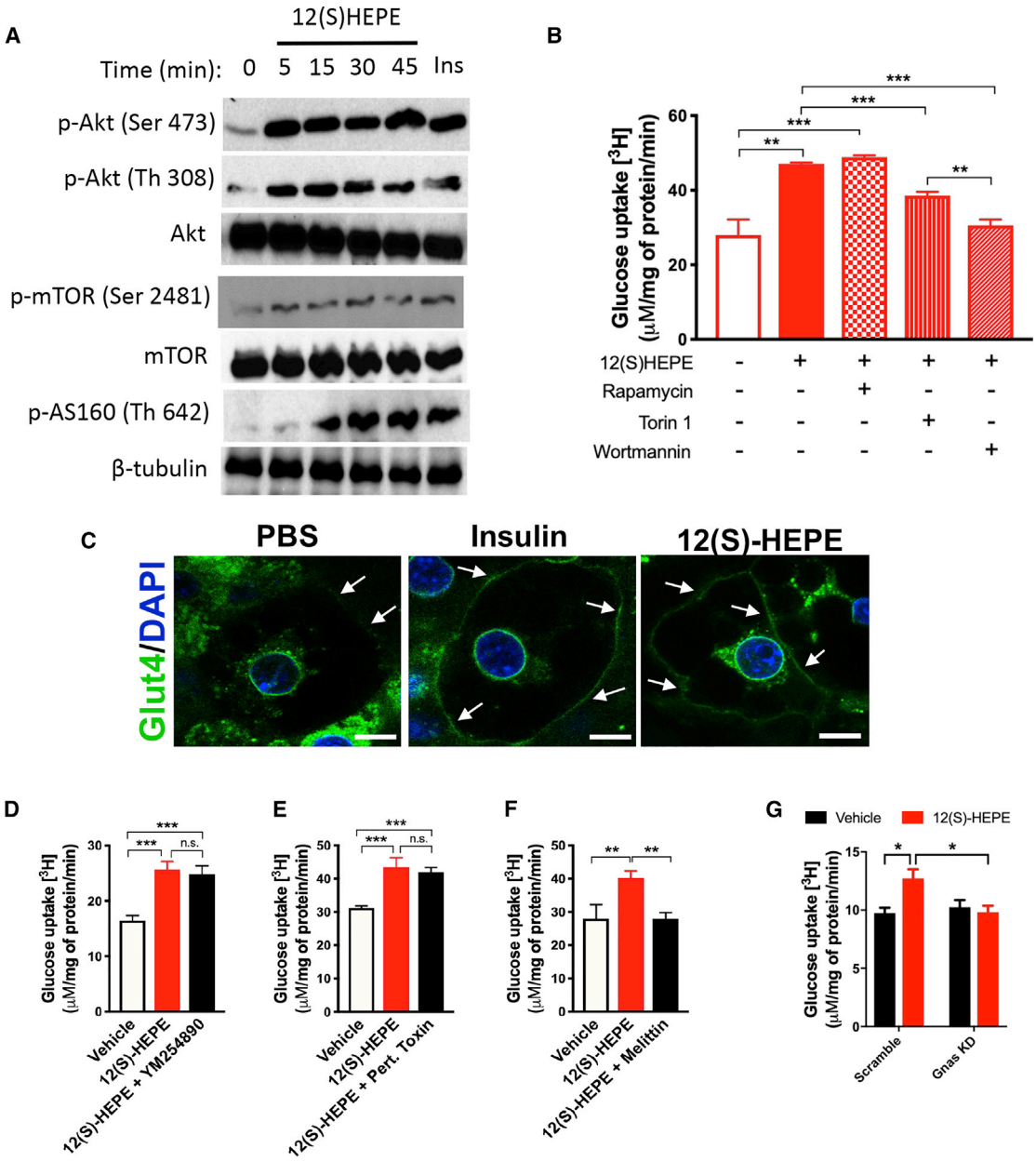

Figure 7. 12-HEPE Promotes Glucose Uptake via a G_sPCR-PI3K-AKT Axis

(A) Western blot analysis of phospho-AKT (Ser473 and Th308), Akt, phospho-mTORC2 (Ser2481), mTOR, phospho-AS160 (Th642), and β-tubulin (loading control) in mouse brown adipocytes treated with 12(S)-HEPE or vehicle.

(B) *In vitro* glucose uptake in murine brown adipocytes treated with 12(S)-HEPE or vehicle in the presence or absence of pre-treatment with rapamycin, Torin 1, or Wortmannin.

(C) Immunofluorescent staining for Glut-4 in murine brown adipocytes treated with PBS, insulin, or 12(S)-HEPE. The white arrows indicate Glut-4 staining in the plasma membrane.

(D–F) *In vitro* glucose uptake in murine brown adipocytes treated with 12(S)-HEPE or vehicle in the presence or absence of pre-treatment with YM254890 (D), pertussis toxin (E), or melittin (F).

(G) *In vitro* glucose uptake in Scramble control or Gnas KD murine brown adipocytes treated with 12(S)-HEPE or vehicle. *$p < 0.05$, **$p < 0.01$, ***$p < 0.001$. Data are represented as mean ± SEM. See also Figure S7.

of type 2 diabetes or obesity by means of biosynthesizing 12-HETE, which leads to impairment of insulin signaling in adipocytes and hinders β-cell function by exerting a pro-inflammatory effect in these tissues (Nunemaker et al., 2008; Ma et al., 2010; Cole et al., 2013; Tersey et al., 2014). 12-LOX whole-body KO mice are protected against high fat diet (HFD)-induced insulin resistance and inflammation (Nunemaker et al., 2008). It is conceivable that under high-fat feeding, lipoxygenase activity

might shift toward the AA cascade when this substrate is more abundant (Brash, 1999; Joshi et al., 2013). Since HFD has an omega-6 to omega-3 ratio approximately 2-fold higher than a regular chow diet, this imbalance results in the increased availability of the pro-inflammatory substrate, which may help to explain the deleterious role of 12-LOX in obesogenic murine models. Here, we show that 12-LOX activity, specifically in BAT, has important implications for glucose metabolism and thermoregulation. Deletion of 12-LOX in brown adipocytes *in vitro* and *in vivo* results in impaired glucose uptake and glycolysis, as well as cold intolerance. These results suggest that 12-LOX may play tissue-specific roles by producing distinct metabolites, which may explain in part the seemly conflicting results between the previously reported whole body KO mice and the brown-fat-specific KO model described in the current study.

Although we demonstrate that brown adipocytes produce 12-HEPE and release it into the circulation, one cannot neglect that other cell types, such as white adipocytes, platelets, or myeloid cells, could also contribute to circulating levels of 12-LOX metabolites, since 12-LOX is abundantly expressed in these cell types (Deng et al., 2014; Serhan, 2014; Kuhn et al., 2015). However, by combining both serum and tissue lipidomics in normal C57BL/6 mice and a mouse model with BAT paucity with the *ex vivo* and *in vitro* studies, we demonstrate that 12-HEPE is a cold-induced 12-LOX metabolite that is produced and released from BAT. Surprisingly, we find that the release of all three 12-LOX products is blunted in the $UCP1^{CRE}$/Alox12 KO mice in response to an acute cold challenge, suggesting that, in addition to 12-HEPE, 14-HDHA and 12-HETE may also be released from BAT in response to acute cold exposure. Whether such changes are sustained in prolonged cold acclimatization warrants future investigations.

Recently, emerging evidence suggests that both shivering and non-shivering thermogenesis contribute to defending body temperature upon acute cold challenges. First, it is well known that the UCP1-KO mice are cold intolerant when directly transferred from room temperature to cold environment (Enerbäck et al., 1997). In addition, transgenic mouse models with impaired brown fat activity also display compromised adaptation to acute cold exposure (Schulz et al., 2013; Ohno et al., 2013). Importantly, data from the current study demonstrate that BAT-derived lipid mediators play an essential role in acute cold tolerance presumably via enhancing non-shivering thermogenesis. Additionally, the data from our $Adipoq^{CRE}/Atgl^{flox}$ KO mice indicate that upon acute cold exposure, lipolysis combined with enhanced 12-LOX activity regulates the secretion of 12-LOX oxylipins into the circulation. Interestingly, it has been recently shown that ATGL-mediated lipolysis in BAT is dispensable for cold adaptation, but adequate nutrient supply is important for proper thermoregulation (Schreiber et al., 2017). It is possible that ATGL-dependent lipolysis in WAT can also contribute to the acute release of 12-LOX metabolites and other lipid substrates for adaptive thermogenesis. This establishes a cross-talk between WAT and BAT via the release of lipid mediators in defending body temperature upon cold challenge.

It has been well established that cold and β3-adrenergic stimulation promote BAT glucose uptake and trigger adaptive thermogenesis (van Marken Lichtenbelt et al., 2009; Virtanen et al., 2009; Cypess et al., 2015). Moreover, the β3-adrenergic-mediated glucose uptake in brown adipocytes is known to also rely on a PI3K-mTORC2-Akt pathway (Albert et al., 2016), which reinforces the link between G_sPCR and this signaling pathway in brown fat. The exact mechanism by which glucose supports thermogenesis remains unclear, although it has been shown that BAT glucose uptake and subsequent glycolysis in response to cold are required to compensate for the loss of mitochondrial ATP production due to mitochondrial uncoupling (Vallerand et al., 1990). In addition, glucose is needed for anaplerotic reactions to maintain fatty acid oxidation (Hao et al., 2015), and triggers *de novo* lipogenesis, which in turn provides fatty acids for UCP1 activation (Sanchez-Gurmaches et al., 2018). In agreement with these findings, 12-LOX protein expression is induced by cold in BAT, and its metabolite 12-HEPE can increase the expression of *de novo* lipogenesis genes and Glut-1 in BAT, promote Glut-4 translocation to the plasma membrane and ultimately increase glucose uptake into brown adipocytes. These data provide important mechanistic insights linking cold-induced glucose uptake and adaptive thermogenesis.

Our study reveals a novel role of 12-LOX in adaptive thermogenesis and glucose utilization. We demonstrate that 12-LOX activity in BAT is indispensable for cold tolerance, presumably by biosynthesizing and releasing the orphan lipid mediator 12-HEPE. 12-HEPE then acts as an autocrine and endocrine factor to promote glucose uptake into BAT and skeletal muscle through activation of the PI3K-mTOR-Akt-Glut pathway. Given the non-toxic nature of the lipid, the observed metabolic effects and the mechanisms of action elucidated in our study, 12-HEPE, or 12-HEPE-mimetics, holds great therapeutic potential for reducing hyperglycemia in diabetic patients. Taken together, our data not only reveal a previously unrecognized mechanism coupling lipid oxidation and adaptive thermogenesis but also provide new therapeutic approaches for individuals with diabetes and other related metabolic disorders.

Limitations of Study

In this study, we have described a mechanism regulating cold adaptation through a coordinated biosynthesis and release of bioactive 12-LOX metabolites from BAT into the circulation. Although we have chosen to study the role of the EPA-derived lipid mediator,12-HEPE, on the regulation of nutrient metabolism, the contributions of the other two metabolites, namely 12-HETE and 14-HDHA, to cold acclimatization and fuel utilization remain to be determined. Furthermore, mechanisms linking 12-HEPE-induced glucose uptake and thermoregulation in brown adipocytes also warrant future investigations. Finally, a thorough pharmacokinetic characterization of 12-HEPE, as well as the identification of its putative receptor, will enhance the understanding of 12-HEPE's action and contribute to the development of 12-HEPE-based therapies in treating metabolic diseases.

STAR★METHODS

Detailed methods are provided in the online version of this paper and include the following:

- KEY RESOURCES TABLE
- LEAD CONTACT AND MATERIALS AVAILABILITY

- EXPERIMENTAL MODEL AND SUBJECT DETAILS
  - Mice and Treatments
  - Study with Human Subjects Treated with Mirabegron
  - Study with Obese and Lean Human Subjects
  - Generation of Alox12 KO Cells
  - Generation of UCP1^{CRE}/Alox12 KO Mice
- METHOD DETAILS
  - Preparation of 12(S)-HEPE
  - Cold Tolerance Tests
  - *In Vivo* Thermogenic Capacity through Indirect Calorimetry
  - Glucose and Insulin Tolerance Tests
  - *In Vivo* Glucose Uptake
  - Signaling Lipidomics
  - Targeted Lipidomics
  - *In Vitro* Glucose Uptake
  - Glut-4 Translocation
  - mRNA Expression
  - Protein expression
  - Cellular Bioenergetic Profile
  - Oil Red O Staining
  - Flow Cytometry
- QUANTIFICATION AND STATISTICAL ANALYSIS
- DATA AND CODE AVAILABILITY

SUPPLEMENTAL INFORMATION

Supplemental Information can be found online at https://doi.org/10.1016/j.cmet.2019.07.001.

ACKNOWLEDGMENTS

This work was supported in part by US National Institutes of Health (NIH) grants R01DK077097 and R01DK102898 (to Y.-H.T.); R01HL106173 and P01GM095467 (to M.S.); R01DK099511 (to L.J.G.) and P30DK036836 (to Joslin Diabetes Center's Diabetes Research Center) from the National Institute of Diabetes and Digestive and Kidney Diseases; and by US Army Medical Research grant W81XWH-17-1-0428 (to Y.-H.T.). L.O.L. was supported by an American Diabetes Association post-doctoral fellowship (1-16-PDF-063) and by the São Paulo Research Foundation (FAPESP) grant 2017/02684. M.D.L. was supported by NIH grants T32DK007260, F32DK102320, and K01DK111714. K.v.L. was supported by the grant R21NS087165. A.B. was supported by a Deutsche Forschungsgemeinschaft research fellowship (BA 4925/1-1) and the Deutsches Zentrum für Herz-Kreislauf-Forschung. B.E.S. is supported by an NRSA from the NIH (HL136044). We thank A. Clermont, A. Dean, and K. Longval of the Joslin Diabetes Center Physiology core. We also would like to thank Dr. Fabio Tucci of Epigen Biosciences, San Diego, who synthesized LOXBlock-1. We apologize to colleagues whose work we could not cite due to space limitations.

AUTHOR CONTRIBUTIONS

L.O.L. and Y.-H.T. conceived the study and designed and supervised the experiments. C.H.W. generated *Gnas* and *Alox12* KD cells and performed bioenergetic profile and glucose uptake experiments in these cells. C.H.W. performed immunofluorescence studies. L.O.L., K.Y., and C.H.W. performed the western blottings in tissues and cells. L.O.L. and F.S. generated the Adipo^{CRE}-Alox12 KO mice. L.O.L., C.H.W., M.D.L., F.S., M.S., S.S., T.L.L., J.D., and A.B. planned and performed *in vivo* glucose uptake. L.O.L. and K.Y. performed *in vitro* glucose uptake. L.O.L. and F.S. performed the indirect calorimetry *in vivo* studies. L.O.L. and K.Y. performed the *in vivo* physiologic studies such as GTT, ITT, and cold tolerance tests. E.Y.C., V.B., N.R.N., and M.A.K. planned and performed the global lipidomics. B.E.S. and M.S. planned and performed the targeted lipidomics. S.D.K. performed the 12-HEPE injections for its quantification in plasma. M.S. performed the flow cytometry experiments. L.O.L. and A.L.R. ran the qPCR experiments in adipose tissues, adipocyte, and SVF fractions. T.J.S. generated Myf5^{+CRE}/Bmpr1a^{flox}. K.v.L. helped design the experiments with 12-LOX-inhibitors. M.B. provided serum samples from obese, overweight, and lean patients. A.M.C. provided plasma samples from mirabegron-treated human volunteers. L.J.G., M.D.L., G.S.H., M.F.H., M.A.K., M.S., A.B., and K.v.L. helped with discussion and interpretation of results. L.O.L and Y.-H.T. wrote the manuscript.

DECLARATION OF INTERESTS

E.Y.C., V. B., N.R.N., and M.A.K. are employees of BERG.

Received: July 12, 2018
Revised: March 12, 2019
Accepted: July 1, 2019
Published: July 25, 2019

REFERENCES

Ahmadian, M., Abbott, M.J., Tang, T., Hudak, C.S., Kim, Y., Bruss, M., Hellerstein, M.K., Lee, H.Y., Samuel, V.T., Shulman, G.I., et al. (2011). Desnutrin/ATGL is regulated by AMPK and is required for a brown adipose phenotype. Cell Metab. *13*, 739–748.

Albert, V., Svensson, K., Shimobayashi, M., Colombi, M., Muñoz, S., Jimenez, V., Handschin, C., Bosch, F., and Hall, M.N. (2016). mTORC2 sustains thermogenesis via Akt-induced glucose uptake and glycolysis in brown adipose tissue. EMBO Mol. Med. *8*, 232–246.

Barquissau, V., Ghandour, R.A., Ailhaud, G., Klingenspor, M., Langin, D., Amri, E.Z., and Pisani, D.F. (2017). Control of adipogenesis by oxylipins, GPCRs and PPARs. Biochimie *136*, 3–11.

Bartelt, A., Bruns, O.T., Reimer, R., Hohenberg, H., Ittrich, H., Peldschus, K., Kaul, M.G., Tromsdorf, U.I., Weller, H., Waurisch, C., et al. (2011). Brown adipose tissue activity controls triglyceride clearance. Nat. Med. *17*, 200–205.

Bartelt, A., Widenmaier, S.B., Schlein, C., Johann, K., Goncalves, R.L.S., Eguchi, K., Fischer, A.W., Parlakgül, G., Snyder, N.A., Nguyen, T.B., et al. (2018). Brown adipose tissue thermogenic adaptation requires Nrf1-mediated proteasomal activity. Nat. Med. *24*, 292–303.

Baskin, A.S., Linderman, J.D., Brychta, R.J., McGehee, S., Anflick-Chames, E., Cero, C., Johnson, J.W., O'Mara, A.E., Fletcher, L.A., Leitner, B.P., et al. (2018). Regulation of human adipose tissue activation, gallbladder size, and bile acid metabolism by a β3-adrenergic receptor agonist. Diabetes *67*, 2113–2125.

Bonadonna, R.C., Del Prato, S., Saccomani, M.P., Bonora, E., Gulli, G., Ferrannini, E., Bier, D., Cobelli, C., and DeFronzo, R.A. (1993). Transmembrane glucose transport in skeletal muscle of patients with non-insulin-dependent diabetes. J. Clin. Invest. *92*, 486–494.

Brash, A.R. (1999). Lipoxygenases: occurrence, functions, catalysis, and acquisition of substrate. J. Biol. Chem. *274*, 23679–23682.

Cannon, B., and Nedergaard, J. (2004). Brown adipose tissue: function and physiological significance. Physiol. Rev. *84*, 277–359.

Cao, H., Gerhold, K., Mayers, J.R., Wiest, M.M., Watkins, S.M., and Hotamisligil, G.S. (2008). Identification of a lipokine, a lipid hormone linking adipose tissue to systemic metabolism. Cell *134*, 933–944.

Capdevila, J.H., Wang, W., and Falck, J.R. (2015). Arachidonic acid monooxygenase: Genetic and biochemical approaches to physiological/pathophysiological relevance. Prostaglandins Other Lipid Mediat. *120*, 40–49.

Chen, Y., Buyel, J.J., Hanssen, M.J., Siegel, F., Pan, R., Naumann, J., Schell, M., van der Lans, A., Schlein, C., Froehlich, H., et al. (2016). Exosomal microRNA miR-92a concentration in serum reflects human brown fat activity. Nat. Commun. *7*, 11420.

Chouchani, E.T., Kazak, L., Jedrychowski, M.P., Lu, G.Z., Erickson, B.K., Szpyt, J., Pierce, K.A., Laznik-Bogoslavski, D., Vetrivelan, R., Clish, C.B., et al. (2016). Mitochondrial ROS regulate thermogenic energy expenditure and sulfenylation of UCP1. Nature *532*, 112–116.

Cole, B.K., Lieb, D.C., Dobrian, A.D., and Nadler, J.L. (2013). 12- and 15-lipoxygenases in adipose tissue inflammation. Prostaglandins Other Lipid Mediat. *104–105*, 84–92.

Cypess, A.M., Lehman, S., Williams, G., Tal, I., Rodman, D., Goldfine, A.B., Kuo, F.C., Palmer, E.L., Tseng, Y.H., Doria, A., et al. (2009). Identification and importance of brown adipose tissue in adult humans. N. Engl. J. Med. *360*, 1509–1517.

Cypess, A.M., Weiner, L.S., Roberts-Toler, C., Franquet Elía, E., Kessler, S.H., Kahn, P.A., English, J., Chatman, K., Trauger, S.A., Doria, A., et al. (2015). Activation of human brown adipose tissue by a β3-adrenergic receptor agonist. Cell Metab. *21*, 33–38.

Dalli, J., Colas, R.A., Walker, M.E., and Serhan, C.N. (2018). Lipid mediator metabolomics via LC-MS/MS profiling and analysis. Methods Mol. Biol. *1730*, 59–72.

Deng, B., Wang, C.W., Arnardottir, H.H., Li, Y., Cheng, C.Y., Dalli, J., and Serhan, C.N. (2014). Maresin biosynthesis and identification of maresin 2, a new anti-inflammatory and pro-resolving mediator from human macrophages. PLoS One *9*, e102362.

Enerbäck, S., Jacobsson, A., Simpson, E.M., Guerra, C., Yamashita, H., Harper, M.E., and Kozak, L.P. (1997). Mice lacking mitochondrial uncoupling protein are cold-sensitive but not obese. Nature *387*, 90–94.

Ferré, P., Leturque, A., Burnol, A.F., Penicaud, L., and Girard, J. (1985). A method to quantify glucose utilization in vivo in skeletal muscle and white adipose tissue of the anaesthetized rat. Biochem. J. *228*, 103–110.

Frontini, A., and Cinti, S. (2010). Distribution and development of brown adipocytes in the murine and human adipose organ. Cell Metab. *11*, 253–256.

GBD 2015 Obesity Collaborators, Afshin, A., Forouzanfar, M.H., Reitsma, M.B., Sur, P., Estep, K., Lee, A., Marczak, L., Mokdad, A.H., Moradi-Lakeh, M., et al. (2017). Health effects of overweight and obesity in 195 countries over 25 years. N. Engl. J. Med. *377*, 13–27.

Haemmerle, G., Lass, A., Zimmermann, R., Gorkiewicz, G., Meyer, C., Rozman, J., Heldmaier, G., Maier, R., Theussl, C., Eder, S., et al. (2006). Defective lipolysis and altered energy metabolism in mice lacking adipose triglyceride lipase. Science *312*, 734–737.

Hamberg, M. (1980). Transformations of 5,8,11,14,17-eicosapentaenoic acid in human platelets. Biochim. Biophys. Acta *618*, 389–398.

Hanssen, M.J., Hoeks, J., Brans, B., van der Lans, A.A., Schaart, G., van den Driessche, J.J., Jörgensen, J.A., Boekschoten, M.V., Hesselink, M.K., Havekes, B., et al. (2015). Short-term cold acclimation improves insulin sensitivity in patients with type 2 diabetes mellitus. Nat. Med. *21*, 863–865.

Hao, Q., Yadav, R., Basse, A.L., Petersen, S., Sonne, S.B., Rasmussen, S., Zhu, Q., Lu, Z., Wang, J., Audouze, K., et al. (2015). Transcriptome profiling of brown adipose tissue during cold exposure reveals extensive regulation of glucose metabolism. Am. J. Physiol. Endocrinol. Metab. *308*, E380–E392.

Joshi, N., Hoobler, E.K., Perry, S., Diaz, G., Fox, B., and Holman, T.R. (2013). Kinetic and structural investigations into the allosteric and pH effect on the substrate specificity of human epithelial 15-lipoxygenase-2. Biochemistry *52*, 8026–8035.

Kajimura, S., Spiegelman, B.M., and Seale, P. (2015). Brown and beige fat: physiological roles beyond heat generation. Cell Metab. *22*, 546–559.

Kriszt, R., Arai, S., Itoh, H., Lee, M.H., Goralczyk, A.G., Ang, X.M., Cypess, A.M., White, A.P., Shamsi, F., Xue, R., et al. (2017). Optical visualisation of thermogenesis in stimulated single-cell brown adipocytes. Sci. Rep. *7*, 1383.

Kuhn, H., Banthiya, S., and van Leyen, K. (2015). Mammalian lipoxygenases and their biological relevance. Biochim. Biophys. Acta *1851*, 308–330.

Liu, S., Brown, J.D., Stanya, K.J., Homan, E., Leidl, M., Inouye, K., Bhargava, P., Gangl, M.R., Dai, L., Hatano, B., et al. (2013). A diurnal serum lipid integrates hepatic lipogenesis and peripheral fatty acid use. Nature *502*, 550–554.

Lynes, M.D., Leiria, L.O., Lundh, M., Bartelt, A., Shamsi, F., Huang, T.L., Takahashi, H., Hirshman, M.F., Schlein, C., Lee, A., et al. (2017). The cold-induced lipokine 12,13-diHOME promotes fatty acid transport into brown adipose tissue. Nat. Med. *23*, 631–637.

Ma, K., Nunemaker, C.S., Wu, R., Chakrabarti, S.K., Taylor-Fishwick, D.A., and Nadler, J.L. (2010). 12-lipoxygenase products reduce insulin secretion and beta-cell viability in human islets. J. Clin. Endocrinol. Metab. *95*, 887–993.

Nedergaard, J., Bengtsson, T., and Cannon, B. (2007). Unexpected evidence for active brown adipose tissue in adult humans. Am. J. Physiol. Endocrinol. Metab. *293*, E444–E452.

Nunemaker, C.S., Chen, M., Pei, H., Kimble, S.D., Keller, S.R., Carter, J.D., Yang, Z., Smith, K.M., Wu, R., Bevard, M.H., et al. (2008). 12-Lipoxygenase-knockout mice are resistant to inflammatory effects of obesity induced by Western diet. Am. J. Physiol. Endocrinol. Metab. *295*, E1065–E1075.

Oh, D.Y., Talukdar, S., Bae, E.J., Imamura, T., Morinaga, H., Fan, W., Li, P., Lu, W.J., Watkins, S.M., and Olefsky, J.M. (2010). GPR120 is an omega-3 fatty acid receptor mediating potent antiinflammatory and insulin-sensitizing effects. Cell *142*, 687–698.

Ohno, H., Shinoda, K., Ohyama, K., Sharp, L.Z., and Kajimura, S. (2013). EHMT1 controls brown adipose cell fate and thermogenesis through the PRDM16 complex. Nature *504*, 163–167.

Platt, R.J., Chen, S., Zhou, Y., Yim, M.J., Swiech, L., Kempton, H.R., Dahlman, J.E., Parnas, O., Eisenhaure, T.M., Jovanovic, M., et al. (2014). CRISPR-Cas9 knockin mice for genome editing and cancer modeling. Cell *159*, 440–455.

Roberto, C.A., Swinburn, B., Hawkes, C., Huang, T.T., Costa, S.A., Ashe, M., Zwicker, L., Cawley, J.H., and Brownell, K.D. (2015). Patchy progress on obesity prevention: emerging examples, entrenched barriers, and new thinking. Lancet *385*, 2400–2409.

Sahu, B.D., Mahesh Kumar, J., and Sistla, R. (2015). Baicalein, a bioflavonoid, prevents cisplatin-induced acute kidney injury by up-regulating antioxidant defenses and down-regulating the MAPKs and NF-κB pathways. PLoS One *10*, e0134139.

Sanchez-Gurmaches, J., Tang, Y., Jespersen, N.Z., Wallace, M., Martinez Calejman, C., Gujja, S., Li, H., Edwards, Y.J.K., Wolfrum, C., Metallo, C.M., et al. (2018). Brown fat AKT2 is a cold-induced kinase that stimulates ChREBP-mediated de novo lipogenesis to optimize fuel storage and thermogenesis. Cell Metab *27*, 195–209.e6.

Sarbassov, D.D., Guertin, D.A., Ali, S.M., and Sabatini, D.M. (2005). Phosphorylation and regulation of Akt/PKB by the rictor-mTOR complex. Science *307*, 1098–1101.

Schreiber, R., Diwoky, C., Schoiswohl, G., Feiler, U., Wongsiriroj, N., Abdellatif, M., Kolb, D., Hoeks, J., Kershaw, E.E., Sedej, S., et al. (2017). Cold-induced thermogenesis depends on ATGL-mediated lipolysis in cardiac muscle, but not brown adipose tissue. Cell Metab. *26*, 753–763.e7.

Schulz, T.J., Huang, P., Huang, T.L., Xue, R., McDougall, L.E., Townsend, K.L., Cypess, A.M., Mishina, Y., Gussoni, E., and Tseng, Y.H. (2013). Brown-fat paucity due to impaired BMP signalling induces compensatory browning of white fat. Nature *495*, 379–383.

Seale, P., Bjork, B., Yang, W., Kajimura, S., Chin, S., Kuang, S., Scimè, A., Devarakonda, S., Conroe, H.M., Erdjument-Bromage, H., et al. (2008). PRDM16 controls a brown fat/skeletal muscle switch. Nature *454*, 961–967.

Serhan, C.N. (2014). Pro-resolving lipid mediators are leads for resolution physiology. Nature *510*, 92–101.

Serhan, C.N., Yang, R., Martinod, K., Kasuga, K., Pillai, P.S., Porter, T.F., Oh, S.F., and Spite, M. (2009). Maresins: novel macrophage mediators with potent antiinflammatory and proresolving actions. J. Exp. Med. *206*, 15–23.

Shi, L., Hao, Z., Zhang, S., Wei, M., Lu, B., Wang, Z., and Ji, L. (2018). Baicalein and baicalin alleviate acetaminophen-induced liver injury by activating Nrf2 antioxidative pathway: the involvement of ERK1/2 and PKC. Biochem. Pharmacol. *150*, 9–23.

Shin, H., Ma, Y., Chanturiya, T., Cao, Q., Wang, Y., Kadegowda, A.K.G., Jackson, R., Rumore, D., Xue, B., Shi, H., et al. (2017). Lipolysis in brown adipocytes is not essential for cold-induced thermogenesis in mice. Cell Metab. *26*, 764–777.e5.

Singh, G.M., Danaei, G., Farzadfar, F., Stevens, G.A., Woodward, M., Wormser, D., Kaptoge, S., Whitlock, G., Qiao, Q., Lewington, S., et al. (2013). The age-specific quantitative effects of metabolic risk factors on cardiovascular diseases and diabetes: a pooled analysis. PLoS One *8*, e65174.

Spite, M., Clària, J., and Serhan, C.N. (2014). Resolvins, specialized proresolving lipid mediators, and their potential roles in metabolic diseases. Cell Metab. *19*, 21–36.

Stanford, K.I., Lynes, M.D., Takahashi, H., Baer, L.A., Arts, P.J., May, F.J., Lehnig, A.C., Middelbeek, R.J.W., Richard, J.J., So, K., et al. (2018). 12,13-diHOME: an exercise-induced lipokine that increases skeletal muscle fatty acid uptake. Cell Metab. *27*, 1111–1120.e3.

Stanford, K.I., Middelbeek, R.J.W., Townsend, K.L., An, D., Nygaard, E.B., Hitchcox, K.M., Markan, K.R., Nakano, K., Hirshman, M.F., Tseng, Y.H., et al. (2013). Brown adipose tissue regulates glucose homeostasis and insulin sensitivity. J. Clin. Invest. *123*, 215–223.

Talukdar, S., Olefsky, J.M., and Osborn, O. (2011). Targeting GPR120 and other fatty acid-sensing GPCRs ameliorates insulin resistance and inflammatory diseases. Trends Pharmacol. Sci. *32*, 543–550.

Tersey, S.A., Maier, B., Nishiki, Y., Maganti, A.V., Nadler, J.L., and Mirmira, R.G. (2014). 12-lipoxygenase promotes obesity-induced oxidative stress in pancreatic islets. Mol. Cell. Biol. *34*, 3735–3745.

Townsend, K.L., and Tseng, Y.H. (2014). Brown fat fuel utilization and thermogenesis. Trends Endocrinol. Metab. *25*, 168–177.

Tseng, Y.H., Kriauciunas, K.M., Kokkotou, E., and Kahn, C.R. (2004). Differential roles of insulin receptor substrates in brown adipocyte differentiation. Mol. Cell. Biol. *24*, 1918–1929.

Vallerand, A.L., Pérusse, F., and Bukowiecki, L.J. (1990). Stimulatory effects of cold exposure and cold acclimation on glucose uptake in rat peripheral tissues. Am. J. Physiol. *259*, R1043–R1049.

van der Lans, A.A., Hoeks, J., Brans, B., Vijgen, G.H., Visser, M.G., Vosselman, M.J., Hansen, J., Jörgensen, J.A., Wu, J., Mottaghy, F.M., et al. (2013). Cold acclimation recruits human brown fat and increases nonshivering thermogenesis. J. Clin. Invest. *123*, 3395–3403.

van Marken Lichtenbelt, W.D., Vanhommerig, J.W., Smulders, N.M., Drossaerts, J.M.A.F.L., Kemerink, G.J., Bouvy, N.D., Schrauwen, P., and Teule, G.J.J. (2009). Cold-activated brown adipose tissue in healthy men. N. Engl. J. Med. *360*, 1500–1508.

Vegiopoulos, A., Müller-Decker, K., Strzoda, D., Schmitt, I., Chichelnitskiy, E., Ostertag, A., Berriel Diaz, M., Rozman, J., Hrabe de Angelis, M., Nüsing, R.M., et al. (2010). Cyclooxygenase-2 controls energy homeostasis in mice by de novo recruitment of brown adipocytes. Science *328*, 1158–1161.

Villarroya, F., Cereijo, R., Villarroya, J., and Giralt, M. (2017). Brown adipose tissue as a secretory organ. Nat. Rev. Endocrinol. *13*, 26–35.

Virtanen, K.A., Lidell, M.E., Orava, J., Heglind, M., Westergren, R., Niemi, T., Taittonen, M., Laine, J., Savisto, N.J., Enerbäck, S., et al. (2009). Functional brown adipose tissue in healthy adults. N. Engl. J. Med. *360*, 1518–1525.

Wang, G.X., Zhao, X.Y., and Lin, J.D. (2015). The brown fat secretome: metabolic functions beyond thermogenesis. Trends Endocrinol. Metab. *26*, 231–237.

Wang, G.X., Zhao, X.Y., Meng, Z.X., Kern, M., Dietrich, A., Chen, Z., Cozacov, Z., Zhou, D., Okunade, A.L., Su, X., et al. (2014). The brown fat-enriched secreted factor Nrg4 preserves metabolic homeostasis through attenuation of hepatic lipogenesis. Nat. Med. *20*, 1436–1443.

Xue, R., Lynes, M.D., Dreyfuss, J.M., Shamsi, F., Schulz, T.J., Zhang, H., Huang, T.L., Townsend, K.L., Li, Y., Takahashi, H., et al. (2015). Clonal analyses and gene profiling identify genetic biomarkers of the thermogenic potential of human brown and white preadipocytes. Nat. Med. *21*, 760–768.

Yigitkanli, K., Pekcec, A., Karatas, H., Pallast, S., Mandeville, E., Joshi, N., Smirnova, N., Gazaryan, I., Ratan, R.R., Witztum, J.L., et al. (2013). Inhibition of 12/15-lipoxygenase as therapeutic strategy to treat stroke. Ann. Neurol. *73*, 129–135.

Yoneshiro, T., Aita, S., Matsushita, M., Kayahara, T., Kameya, T., Kawai, Y., Iwanaga, T., and Saito, M. (2013). Recruited brown adipose tissue as an antiobesity agent in humans. J. Clin. Invest. *123*, 3404–3408.

Yore, M.M., Syed, I., Moraes-Vieira, P.M., Zhang, T., Herman, M.A., Homan, E.A., Patel, R.T., Lee, J., Chen, S., Peroni, O.D., et al. (2014). Discovery of a class of endogenous mammalian lipids with anti-diabetic and anti-inflammatory effects. Cell *159*, 318–332.

STAR★METHODS

KEY RESOURCES TABLE

REAGENT or RESOURCE	SOURCE	IDENTIFIER
Antibodies		
Phospho-Akt (Ser473)	Cell Signaling Technology	Cat# 9271
Phospho-Akt (Thr308)	Cell Signaling Technology	Cat# 13038
Akt	Cell Signaling Technology	Cat# 4685; RRID: AB_2225340
Phospho-mTOR (Ser2481)	Cell Signaling Technology	Cat# 2974; RRID: AB_2262884
mTOR (7C10)	Cell Signaling Technology	Cat# 2983; RRID: AB_10693786
Phospho-AS160 (Thr642)	Cell Signaling Technology	Cat# 8881; RRID: AB_2651042
Beta-tubulin	Cell Signaling Technology	Cat# 2146; RRID: AB_10694206
Actin	Millipore	Cat# MAB1501R; RRID: AB_2223041
12-LO Antibody (C5)	Santa Cruz Biotechnology	Cat# sc-365194; RRID: AB_10709144
CD45-PE-Cy7	eBiosciences	Cat# 25-0451-82
F4/80-APC-Cy7	BioLegend	Cat# 123118
CD206-Alex647	BioRad	Cat# MCA2235A647
CD11c-PE	BD Pharmingen	Cat# 561044
Chemicals, Peptides and Recombinant Proteins		
12(S)-HEPE	Cayman Chemicals	Cat# 32550
Insulin (adipocytes differentiation)	Sigma Aldrich	Cat# I6634
Insulin (human, for glucose uptake)	Sigma Aldrich	Cat# I9278
Insulin (Humulin, for ITT))	Elly Lilli	N/A
NCTT956	Sigma Aldrich	Cat# SML0499
Norepinephrine	Sigma Aldrich	Cat# A0937
Rosiglitazone	Sigma Aldrich	Cat# R2408
Indomethacin	Sigma Aldrich	Cat# I7378
Dexamethasone	Sigma Aldrich	Cat# D4902
IBMX	Sigma Aldrich	Cat# I5879
Rotenone	Sigma Aldrich	Cat# R8875
Antimycin A	Sigma Aldrich	Cat# A8674
FCCP	Sigma Aldrich	Cat# C2920
Oligomycin	Millipore	Cat# 495455
$ZnSO_4$	Sigma Aldrich	Cat# Z2876
$Ba(OH)_2$	Sigma Aldrich	Cat# B4059
Perchloric acid	Sigma Aldrich	Cat# 244252
Pertussis toxin	Sigma Aldrich	Cat# P7208
Bacalein	Tocris	Cat# 1761
Melittin	Tocris	Cat# 1193
CL316,243	Tocris	Cat# 1499
YM254890	FujiFilm Wako Chemicals	Cat# 257-00631
LOXBlock-1	Donated by Epigen Biosciences	N/A
[^{3}H]2-deoxyglucose	Perkin Elmer	Cat# 760562
Critical Commercial Assays		
Insulin Kit	Cristal Chemicals	Cat# 90080
Cell Line Nucleofector kit	Lonza	Cat# VVCA-1003
Pierce BCA Protein Assay kit	Thermo Fisher	Cat# 23225

(*Continued on next page*)

Continued

REAGENT or RESOURCE	SOURCE	IDENTIFIER
RNA extraction kit	Zymo Research	Cat# R2052
Sybr Green Master Mix	Thermo Fisher	Cat# A25778
cDNA Reverse Transcription Kit	Thermo Fisher	Cat# 4368813
Oligonucleotides		
Primers for qPCR	See Table S1 – this paper	N/A
Primers for gRNAs	See Method Details – this paper	N/A
Gnas siRNA	Dharmacon	Cat# R040646-00-0005
Control siRNA	Dharmacon	Cat# D-001810-10-05
Recombinant DNA		
Alox 12 Myc-DDK-tagged	Origene	Cat# MR227302
1179_pAAV-U6-BbsI-gRNA-CB-EmGFP	Addgene	Cat# 89060
pSpCas9(BB)-2A-Puro (PX459) V2.0	Addgene	Cat# 62988
Experimental Models: Cell Lines		
WT-1 cells	Developed in Tseng lab	Tseng et al., 2004
hWA A41	Developed in Tseng lab	Xue et al., 2015; Kriszt et al., 2017
hBA A41	Developed in Tseng lab	Xue et al., 2015; Kriszt et al., 2017
C2C12	ATCC	Cat# CRL-1772
3T3-F442A	Sigma	Cat# 00070654
Experimental Models: Organisms/Strains		
C57BL6/J	Jackson Laboratories	Cat# 000664
Atgl FLOX	Jackson Laboratories	Cat# 024278
Cas9 knockin mice	Jackson Laboratories	Cat# 024857
Myf5+ CRE	Jackson Laboratories	Cat# 007893
STOCK Bmpr1a$^{tm2.1Bhr}$ /Mmnc	MMRRC	Cat# 030469-UNC
Ucp1-CRE	Jackson Laboratories	Cat# 024670
Adiponectin-CRE	Jackson Laboratories	Cat# 028020
Datasets		
Global Lipidomics Datasets	www.metabolomicsworkbench.org	Project ID: PR000811 (https://doi.org/10.21228/M8VD62). Studies IDs: ST001206; ST001207; ST001213; ST001214; ST001215
Algorithms and Software		
GraphPad Prizm	GraphPad Software, San Diego, CA	Versions 7 and 8
ImageJ	NIH	https://fiji.sc/

LEAD CONTACT AND MATERIALS AVAILABILITY

Further information and requests for resources and reagents should be directed to and will be fulfilled by the Lead Contact, Yu-Hua Tseng (yu-hua.tseng@joslin.harvard.edu). This study did not generate new unique reagents.

EXPERIMENTAL MODEL AND SUBJECT DETAILS

Mice and Treatments

All animal procedures were approved by the Institutional Animal Use and Care Committee at Joslin Diabetes Center. The animals utilized in this study were kept at a conventional animal facility at Joslin Diabetes Center. The experiments were not randomized, except the cold tolerance tests, which were performed in a blinded manner. No statistical method was used to predetermine the sample size for the animals. For all of the *in vivo* studies, in which wild-type mice were used, 11–13-week-old male C57BL/6J mice (Stock no. 000664) were purchased from The Jackson Laboratory. The *in vivo* experiments are described in the sections below.

For acute BAT activation, mice were either sacrificed as control animals kept at room temperature or individually housed at 4°C for 1 hour, then sacrificed for serum and tissue collection, which were subsequently sent for lipidomics analysis. For chronic cold exposure, C57BL/6J mice were individually housed at 5°C or 30°C for 7 days. Both acute and chronic exposures were done by housing the mice in temperature controlled diurnal incubators (Caron Products & Services Inc.) on a 12 hour light/dark cycle with *ad libitum* access to food.

In all experiments, interscapular BAT, inguinal WAT, and serum were collected after sacrifice. All tissues were snap frozen in liquid nitrogen and stored at -80°C while serum was frozen at -20°C. For the lipidomic analyses using the *ex vivo* tissue incubation strategy, interscapular BAT (BAT) and inguinal subcutaneous white adipose tissue (ingWAT) were dissected from 12-week-old male C57BL/6J mice chronically exposed to cold or thermoneutrality (as described above) and incubated at 37°C in 300μl of Krebs-Ringer solution (pH 7.4) for 1 hour, after which the tissue was discarded, and LC-MS/MS was performed on the conditioned Krebs solution.

Transgenic mice carrying floxed alleles of BMP receptor 1A (*Bmpr1a*) were used to generate conditional gene deletion mouse models by intercrossing with Myf5-driven cre recombinase and compared to cre-negative littermate controls as described previously (Schulz et al, 2013). These mice were used for a 2-day cold exposure experiment, in which their serum was collected and processed for global lipidomics analysis.

The same intercrossing strategy was used to delete *Atgl* in mouse adipose tissues. *Atgl* floxed mice were crossed (Stock no. 024278, The Jackson Laboratory), with the Adipoq^{CRE} strain (Stock no. 028020, The Jackson Laboratory). As these animals are cold intolerant, they were used only for the acute (1h) cold exposure experiments.

For the experiments with daily injections of 12(S)-HEPE in high-fat diet induced obese (DIO) mice, 6-week-old C57BL/6J were fed with a high-fat diet containing 60 % kcal fat (Research Diets Stock no. D12492) for 16 weeks prior to treatment and during the course of the experiment. Mice were injected intraperitoneally daily with 200μg/kg body weight of 12(S)-HEPE diluted in PBS solution or with vehicle (PBS). Body weight and food intake were monitored. Serum was collected, and glucose (Infinity® Blood Glucose Meter, US Diagnostics), and insulin (Ultra-Sensitive Mouse Insulin ELISA Kit, Crystal Chem), were measured. All mice were allowed *ad libitum* access to water and food. To measure the glucose-induced insulin release, we collected additional blood from the tail at the time 0 and 45min after the glucose IP injection (2g/kg) during the glucose tolerance test.

For indirect calorimetry, PBS or 12(S)-HEPE treated DIO mice were individually housed in metabolic cages of a Comprehensive Lab Animal Monitoring System (CLAMS) at room temperature. After a 12h acclimation period, animals were monitored for 24h in order to obtain measurements for the volume of oxygen consumption (VO_2), the volume of carbon dioxide production (VCO_2) and respiratory exchange ratio (RER), which was calculated as the ratio of total VCO_2 produced to total VO_2 consumed.

Study with Human Subjects Treated with Mirabegron

Human plasma was acquired from a previously performed clinical trial (Cypess et al., 2015) registered with ClinicalTrials.gov (NCT01783470) and had the FDA Investigational New Drug (IND) registration number 116246. It was approved by the Human Studies Institutional Review Boards of Beth Israel Deaconess Medical Center (BIDMC) and Joslin Diabetes Center (JDC). Healthy volunteers were recruited through electronic advertisements and provided written informed consent. The subjects were given a single oral dose of mirabegron, 200 mg. Blood samples were collected 180 minutes after oral dosing. 180 minutes is the corresponding T_{max} (time after administration of a drug when the maximum plasma concentration is reached) found for mirabegron in men (Baskin et al., 2018).

Study with Obese and Lean Human Subjects

A cohort of 55 individuals were selected from the Leipzig biobank (42 women and 13 men) to represent a wide range of BMI (17.5–75.4 kg/m2), categories of lean (BMI < 25 kg/m2; n = 15; 4 male (M)/11 female (F)), overweight (BMI 25.1–29.9 kg/m2; n = 13; 4 M/9 F) or obese (BMI > 30 kg/m2; n = 27; 5 M/22 F) and glucose-metabolism parameters (fasting plasma glucose 3.9–13.4 mmol/liter; fasting plasma insulin 3.8–451 pmol/liter, HOMA-IR: 0.1–25). In the subgroup of lean, all individuals were normal glucose tolerant (NGT), whereas in the overweight subgroup, 10 individuals with NGT and 3 with type 2 diabetes (T2D), and in the obese group, 20 NGT individuals and 7 individuals with T2D were included. Collection of human biomaterial, serum analyses and phenotyping were approved by the ethics committee of the University of Leipzig (approval numbers: 159-12-21052012 and 017-12-23012012), and all individuals gave written informed consent before taking part in the study.

Generation of Alox12 KO Cells

To generate a loss of function model for Alox12 *in vivo*, four different guide RNAs (gRNAs) were designed to target exon 1, 2, or 3 of the mouse *Alox12* gene: gRNA1- GGGCCGCTACCGCGTCCGTG (exon 1); gRNA2 – TACCGCGTCCGTGTGGTCAC (exon 1); gRNA3 – GTTTGACTTCGACGTTCCCG (exon 2); gRNA4 – GAAGTATCGAGAAAAGGAAC (exon 4). The gRNAs were cloned into the pSpCas9(BB)-2A-Puro (PX459) V2.0 plasmid (Addgene plasmid #62988). Backbone and Alox12 gRNA were delivered into mouse preadipocytes (DE cells) through the nucleofection method (Nucleofector™ Technology, Lonza). After 6 days of puromycin selection, stable knockdown mouse preadipocytes were established and then used for adipocyte differentiation and functional experiments. Since gRNA number 2 showed the best efficiency in deleting Alox12 in immortalized brown adipocytes (Figure S3D), future *in vitro* and *in vivo* studies used this gRNA, which targets exon 1 of the *Alox12* gene.

For re-expression of 12-LOX, WT and Alox12 knockdown mouse preadipocytes received GFP or mouse Alox12 cDNA (Myc-DDK-tagged, catalog # MR227302, Origene) through the aforementioned nucleofection method. One day after nucleofection, the cells underwent adipogenic differentiation for 8 days and, once mature, western blot analysis was done in order to confirm the expected modifications in protein expression.

Generation of UCP1^{CRE}/Alox12 KO Mice

gRNA 2 targeting exon 1 of the mouse Alox12 gene was cloned into the 1179_pAAV-U6-BbsI-gRNA-CB-EmGFP plasmid (Addgene plasmid #89060). The Alox12 gRNA or empty vector were packaged in AAV2/8 particles and then bilaterally injected into both brown

adipose tissue lobes of 10-weeks old UCP1^{CRE}/Cas9 knockin mice, thus generating the Ucp1^{CRE}-Alox12 KO mice or empty vector (EV) mice. For the injection, mice were anesthetized with 2.5% solution of Avertin (15ul/g BW), and a small vertical incision was made between the scapulae. After the injections, the incision area was immediately closed and sutured. The animals were maintained on a heating pad following the surgery until complete recovery, and then were housed individually. There was a 2-week interval between the surgery and the beginning of the experimental procedures in these mice.

For the generation of the Ucp1^{CRE}/Cas9 knockin mice, we crossed the Ucp1^{cre} strain (Stock no. 024670, The Jackson Laboratories) with the homozygous Rosa26-floxed STOP-Cas9 knockin mice (Stock no. 024857, The Jackson Laboratory). Rosa26-floxed STOP-Cas9 knockin mice have a cre recombinase-dependent expression of Cas9. As a result, we obtained 50% UCP1^{CRE}/Cas9 (HET) knockin mice and half WT/Cas9 (HET), which were injected with AAV/Alox12 gRNA and AAV/EV, respectively, through the method described above. The efficiency of the 12-LOX deletion was confirmed through western blots in BAT and ingWAT.

METHOD DETAILS

Preparation of 12(S)-HEPE

12(S)-HEPE was purchased from Cayman Chemical (Michigan, USA). Due to its instability, the preparation was done immediately before the experiments and following the manufacturer's instructions. 12(S)-HEPE is supplied as a solution in ethanol. To change the solvent, the ethanol was evaporated under a gentle stream of nitrogen and the resulting neat oil was immediately dissolved in PBS, pH 7.2. The aqueous solution was used immediately after reconstitution.

Cold Tolerance Tests

For cold tolerance tests, mice were intraperitoneally injected with 50μl of the 12-LOX inhibitors, Bacalein (50mg/kg), NCTT956 (50mg/kg), LOXBlock-1 (50mg/kg), or DMSO, 15 minutes before placing the mice at 5°C. In another set of experiments, LOXBlock-1 was co-injected with 200 μg/kg of 12(S)-HEPE 15 minutes before starting the cold exposure. Rectal temperature measurements were done using an aRET-3 rectal probe (Physitemp). Bacalein and LOXBlock1 dosages were chosen based on previous publications (Yigitkanli et al., 2013; Sahu et al., 2015; Shi et al., 2018). Since NCTT956 has not been published yet for *in vivo* application, we decided to adopt the same dosage used for the other two inhibitors.

For the interscapular temperature, telemeters recording both temperature and activity (TA11TA-F10; Data Sciences International) were implanted under the skin in the intrascapular space of anesthetized 12-week old C57Bl/6J mice. Mice were maintained on a heating pad following the surgery and then housed individually. Mice were allowed at least 48 hours for recovery before experiments. Temperature and activity data were collected every 5 minutes.

In Vivo Thermogenic Capacity through Indirect Calorimetry

Mice were injected intraperitoneally with Pentobarbital (65 mg/kg). Basal energy expenditure was measured for 30 minutes before stimulation with Norepinephrine (Sigma, 1 mg/kg in 0.9 % w/v NaCl). Energy expenditure was measured using a CLAMS. After norepinephrine injection, we monitored VO_2 for the following 30 minutes.

Glucose and Insulin Tolerance Tests

For the glucose tolerance test (GTT), animals were fasted for 6 hours (7AM to 1PM) with free access to drinking water. A baseline blood sample was collected from the tail of fully conscious mice, followed by i.p. injection of dextrose (2.0 g/kg body weight), and blood was taken from the tail at 15, 30, 45, 60, 90, and 120 minutes after injection. For the insulin tolerance test (ITT), animals were fasted for 6 hours (7AM to 1PM) with free access to drinking water. Baseline blood samples were collected from the tail of fully conscious mice. Insulin (1 U/kg body weight) (Humulin®; Eli Lilly) was administered by i.p. injection, and blood samples were taken from the tail at 15, 30, 45, and 60 minutes after injection. Glucose concentrations were determined from blood using an Infinity® Blood Glucose Meter (US Diagnostics).

In Vivo Glucose Uptake

Glucose uptake *in vivo* was measured as previously described (Bonadonna et al., 1993). Briefly, 12-week-old C57BL6/J mice were fasted for 5 hours (7AM to 11AM) and then retro-orbitally injected with 12(S)HEPE (200ug/Kg) or vehicle (PBS). Mice were anesthetized 15 minutes after the treatments with sodium pentobarbital (85–100 mg/kg mouse body weight, i.p. injection). After 15 minutes, blood was taken from the tail to assess basal glucose concentrations and background radioactivity levels. Then, mice were injected with [^{3}H]2-deoxyglucose-6-P (Perkin Elmer Life and Analytical Science, Waltham, MA) at 0.33 μCi /g body weight, administered via the retro-orbital sinus, and blood samples were taken after 5, 10, 15 and 25 minutes for the determination of glucose and [^{3}H] levels. After the last blood draw, animals were sacrificed by cervical dislocation, and BAT, perigonadal and subcutaneous WAT, liver, soleus, quadriceps and gastrocnemius were harvested and immediately frozen in liquid nitrogen. Accumulation of [^{3}H]2-deoxyglucose-6-P was assessed in tissues using a perchloric acid/$Ba(OH)_2$/$ZnSO_4$ precipitation procedure modified from previous work (Ferré et al., 1985).

Signaling Lipidomics

Tissue samples were homogenized in 0.1x PBS in Omni homogenizing tubes with ceramic beads at 4°C. Aliquots of 100 μL serum or 1mg protein from homogenized tissue (measured by BCA) were taken, depending on the experiment. A mixture of deuterium-labeled

internal standards was added to each aliquot, followed by 3x volume of sample of cold methanol (MeOH). Samples were vortexed for 5 minutes and stored at −20°C overnight. Cold samples were centrifuged at 14,000g for 10 minutes, and the supernatant was then transferred to a new tube and 3 mL of acidified H_2O (pH 3.5) was added to each sample prior to C18 SPE. The methyl formate fractions were collected, dried under nitrogen, and reconstituted in 50 μL MeOH:H_2O (1:1, by vol). Samples were transferred to 0.5 mL tubes and centrifuged at 20,000g at 4°C for 10 minutes. (35ul) of supernatant was transferred to LC–MS/MS vials for analysis using the BERG LC–MS/MS mediator lipidomics platform. Separation of signaling lipids was performed on an Ekspert MicroLC 200 system (Eksigent Technologies) with a Synergi™ Fusion-RP capillary C18 column (150 × 0.5 mm, 4 μm; Phenomenex Inc., Torrance, CA, USA) heated to 40°C. A sample volume of 11 μL was injected at a flow rate of 20 μL/min. Lipids were separated using mobile phases A (100 % H_2O, 0.1 % acetic acid) and B (100 % MeOH, 0.1 % acetic acid) with a gradient starting at 60% B for 0.5 min, steadily increasing to 80% B by 5 min, reaching 95% B by 9 minutes, holding for 1 minute, and then decreasing to 60% B by 12 minutes. MS analysis was performed on a SCIEX TripleTOF® 5600+ system using the HR-MRM strategy consisting of a TOF MS experiment looped with multiple MS/MS experiments. MS spectra were acquired in high-resolution mode (>30,000) using a 100-ms accumulation time per spectrum. Full-scan MS/MS was acquired in high sensitivity mode, with an accumulation time optimized per cycle. Collision energy was set using rolling collision energy with a spread of 15V. The identity of a component was confirmed using PeakView® software (SCIEX), and quantification was performed using MultiQuant™ software (SCIEX). C18SPE cartridges were purchased from Biotage. All solvents were of HPLC or LC-MS/MS grade and were acquired from Sigma-Aldrich, Fisher Scientific, or VWR International.

Global lipidomics was also performed in cell-conditioned media samples. Differentiated human brown and white adipocytes were treated with vehicle (ethanol) or forskolin (10μM). After that, 100 μL of the medium was collected and immediately snap-frozen in liquid nitrogen. In a separate experimental setting, differentiated murine brown adipocytes were stimulated with the β3-adrenergic receptor agonist CL316,243 (1 μM) or its vehicle (PBS), for 4 hours, and after this period 100 μL of the medium was collected and immediately snap-frozen. Lipidomic analysis of these samples was performed detailed above.

Targeted Lipidomics

Targeted LC-MS/MS analysis was done in serum, BAT and ingWAT collected from C57BL6/J mice housed in cold or thermoneutral temperature, and in BAT collected from either lean or DIO mice kept in room temperature. We also detected circulating levels of 12-HEPE at time 0 (zero) and 30 min after 12(S)-HEPE i.p. injections. After collection, the tissues were then minced in ice-cold methanol containing an internal deuterium-labeled standard (d8-5-HETE) used to assess extraction recovery and aid quantification. For media and serum samples, 2-3 volumes of ice-cold methanol containing d8-5-HETE was added and the samples were stored at -80C prior to extraction. Following centrifugation (3,000 rpm), the supernatants were subjected to solid phase extraction and LC-MS/MS analysis, as described in detail in Dalli et al. (2018). Briefly, samples were acidified (pH 3.5) and lipid mediators were extracted by C18 column chromatography with elution in methyl formate, which was then evaporated under a steady stream of N_2 gas. The samples were resuspended in methanol:water (50:50) and injected into a high-performance liquid chromatograph (HPLC, Shimadzu) coupled to a QTrap5500 mass spectrometer (AB Sciex) that was operated in negative ionization mode. Lipid mediators were identified using retention time, specific multiple reaction monitoring (MRM) transitions, and diagnostic MS/MS fragmentation spectra, as compared with authentic standards. The abundance of individual lipid mediators was determined by normalizing to extraction recovery of the internal d8-5-HETE and extrapolation to calibration curves for external standards using synthetic 12-HEPE, 14-HDHA, and 12-HETE (Cayman Chemical).

In Vitro Glucose Uptake

All the *in vitro* glucose uptake assays were performed in differentiated cells, regardless of the cell type. WT-1 and 3T3-F442A cells were differentiated for 9 days according to a standard adipogenic differentiation protocol. Human brown (hBAT) and white adipocytes hWAT were cultured and differentiated for 12 days as previously described (Xue et al., 2015). C2C12 cells were differentiated for 7 days in a DMEM-high glucose with 1% horse serum. Both human and murine brown and white adipocyte cell lines were serum starved in no-glucose DMEM (Gibco; catalog# 11966025), for 4 hours before the treatments. The mature C2C12 cells were serum starved overnight (18 hours) with low-glucose DMEM (Gibco; catalog# 11885084), before the treatments.

The cells were treated with PBS, 12(S)-HEPE (0.01, 0.1 and 1μM) or insulin (1μM) for 30 minutes before starting the glucose transport procedure. Cells were washed once with HEPES Buffered Saline (HBS), which was then completely aspirated. Then, 300μl of transport solution (TS) containing [^{3}H]2-deoxyglucose (0.5 uCi/ml) and 2-deoxyglucose (5mM) diluted in 20mM HBS solution was added. Cells were incubated in this solution for 5 minutes at room temperature, which was then quickly aspirated. An ice-cold stop solution (0.9% Saline) was added and washed, before the addition of 0.5 ml of a 0.05M NaOH solution to the wells. Cells were scraped and homogenized, and the homogenate transferred to fresh scintillation tubes (0.35ml), where it was vigorously mixed with 4ml of liquid scintillation cocktail (CytoScint™- ES Liquid Scintillation Cocktail, MP Biomedicals) before scintillation counting. Protein levels were determined by BCA assay in the remaining homogenate for the normalization of values.

Gnas was transiently knocked down in brown adipocytes in order to generate *Gnas* KD cells and then confirm the requirement of the G_sPCR for the 12(S)-HEPE mediated glucose uptake. Differentiated brown adipocytes were transfected with 50nM of *Gnas* siRNA (Dharmacon®) or with Scrambled control using PolyJet. After 2 days, we proceeded as described above for wild type cells.

Glut-4 Translocation

WT-1 cells were seeded in a chamber cell culture slide and underwent differentiation for 9 days in the same way we described for the *in vitro* glucose uptake experiments. After serum starvation in no-glucose DMEM for 4 hours, differentiated WT-1 cells were treated with PBS, 1 μM insulin, or 1 μM 12-HEPE. 30 minutes later, cells were fixed with 4% paraformaldehyde, followed by incubation in blocking buffer (2.5% BSA, 0.3% Triton X-100 in PBS) at 4°C overnight. Glut-4 protein was stained by anti-Glut-4 antibody (1:500, Millipore) followed by anti-rabbit IgG secondary antibody conjugated with Alexa Fluor 488 (1:1000). 5 ug/ml DAPI solution was used for nucleus staining. The images were captured using a confocal microscope (Zeiss LSM 700).

mRNA Expression

Total RNA was extracted from tissue with Trizol and purified using a spin column kit (Zymo Research). RNA (500 ng-1 μg) was reverse transcribed with a high-capacity complementary DNA (cDNA) reverse transcription kit (Applied Biosystems). Real-time PCR was performed in mouse tissues starting with 10 ng of cDNA and forward and reverse oligonucleotide primers (300 nM each) in a final volume of 10 μl with SYBR green PCR Master Mix (Life Technologies). Fluorescence was determined and analyzed in an ABI Prism 7900 sequence detection system (Applied Biosystems). Acidic ribosomal phosphoprotein P0 (ARBP) expression was used to normalize gene expression.

Protein expression

WT-1 cells were differentiated into mature brown adipocytes according to a standard adipogenic differentiation protocol (Xue et al., 2015). Cells were serum-starved in no-glucose DMEM for 4 hours and then treated with 12(S)-HEPE (1μM) for 5, 15, 30 and 45 minutes or treated with Insulin (1μM), as a positive control for 15 minutes. After that, cells were scraped from tissue-culture plates into RIPA buffer (Boston BioProducts Inc, Ashland, MA) supplemented with protease and proteinase inhibitors cocktails (Sigma-Aldrich, Dallas, TX) and further homogenized for protein detection. Protein concentrations were determined by using the Pierce BCA kit (Life Technologies), according to the manufacturer's instructions. For immunoblots, lysates were diluted into Laemmli buffer and boiled and then loaded onto 10% Tris gels for SDS–PAGE. After complete separation of the proteins, they were transferred onto a PVDF membrane (Amersham Biosciences), blocked in western blocking buffer (Roche), and primary antibodies were applied in blocking buffer overnight at 4°C. After washing 4x for 15 min with TBS-T, secondary antibodies were applied for 1 h in blocking buffer. Membranes were washed again 3x times for 15 min in TBS-T and developed using chemiluminescence (Thermo Fisher). To quantify the bands in scanned immunoblots, regions of interest of identical size were drawn in each lane at the same molecular weight, and integrated pixel density was measured using ImageJ software. β-tubulin was used as an endogenous control for normalization. For the western blots in tissues in response to 12(S)-HEPE, we anesthetized 12 weeks old C57BL6/J mice with Avertin (375mg/kg), opened the visceral cavity and injected 12(S)-HEPE (200μg/kg, 50μl) or PBS via the vena cava. After 10 minutes, mice were sacrificed, and tissues were collected for protein extraction and western blotting. Protein lysates were stored at −80°C until further use. The data are expressed as the average normalized value for each lane, with the error bars representing S.E.M.

Cellular Bioenergetic Profile

Preadipocytes were seeded onto gelatin-coated Seahorse Plates and differentiated according to standard protocols. Cells were serum-starved for 1 hour prior to the beginning of the experiment. The extracellular acidification rate (ECAR) was monitored in a Seahorse XF24 instrument using the standard glycolysis stress test protocol of 3 minutes mix, 2 minutes wait, and 3 minutes measure. For the glycolysis stress test, cells were challenged with Glucose (25 mM), Oligomycin (2μM), and 2-deoxyglucose (100 mM), allowing 4 measurements after each injection. For the oxygen consumption ratio (OCR) measurements, cells were stimulated with Oligomycin (2μM), FCCP (2μM) and antimycin A (2μM), also allowing 4 measurements after each injection.

For the normalization of respiration to protein content, cells were lysed in RIPA buffer and protein concentration was measured using the Pierce BCA kit (Thermo Fisher).

Oil Red O Staining

Cells were washed twice with PBS and fixed with 10% buffered formalin for 30minutes at room temperature. Cells were then stained with a filtered Oil Red O solution (0.5% Oil Red O in isopropyl alcohol) for 2 hours at room temperature, washed several times with distilled water, and then visualized.

Flow Cytometry

SVF was obtained from pgWAT by treatment with 2 mg/mL collagenase (Sigma) for 45 minutes at 37°C. The isolated SVF was resuspended in cold Hank's balanced salt solution (HBSS) with 2% fetal bovine serum (FBS). Cells were incubated with CD45-PE-Cy7 (eBiosciences), F4/80-APC-Cy7 (BioLegend), CD206-Alex647 (Serotec, Inc.) and CD11c-PE (BD Pharmingen) antibodies for 30 minutes in HBSS containing 2% FBS on ice and then washed and resuspended in solution with Sytox Blue (Thermo Scientific). Cells were analyzed on a BD FACS Aria cell sorter after selection by forward scatter and side scatter, followed by exclusion of dead cells with Sytox Blue staining, and analyzed for cell-surface markers. M1 or M2 macrophages were identified as F4/80+/CD11c+/CD206- or F4/80+/CD11c-/CD206+ cells, respectively. The data are shown as the percentage of M1 and M2 macrophages.

QUANTIFICATION AND STATISTICAL ANALYSIS

No statistical method was used to predetermine sample size. The experiments were not blinded, except the cold tolerance tests. All statistics were calculated using Microsoft Excel and GraphPad Prism. Unpaired Student's t-test was done to compare only 2 groups, and paired Student's t-test was used for 2 paired-groups experiments. One-Way ANOVA followed by a Tukey's post-hoc test was done when comparing more than 3 groups. Correlations were established based on Spearman correlation tests, and the Spearman correlation coefficient was provided and the *p-value* calculated. $P<0.05$ was adopted as significant.

DATA AND CODE AVAILABILITY

The lipid datasets generated during this study are available at Metabolomics Workbench (URL: www.metabolomicsworkbench.org;). The accession number for the lipidomic data of Figures 1A–1F reported in this paper is ST001206. The accesion number for the lipidomic data of Figure 2 reported in this paper is ST001215. The accession number for the lipidomic data of Figure 4A reported in this paper is ST001207. The accession number for the lipidomic data of Figure 4D reported in this paper is ST001213. The accession number for the lipidomic data of Figure 5 reported in this paper is ST001214. All these studies are deposited under the Project ID PR000811, https://doi.org/10.21228/M8VD62, in the Metabolomics Workbench repository.